ITP-UU-07/19
SPIN-07/12

(2+1)-Dimensional Quantum Gravity as the Continuum Limit of Causal Dynamical Triangulations

D. Benedetti[a], R. Loll[a], F.Zamponi[b]

[a] *Spinoza Institute and Institute for Theoretical Physics,*
Utrecht University,
Leuvenlaan 4, NL-3584 CE Utrecht, The Netherlands

[b] *Service de Physique Théorique,*
Orme des Merisiers, CEA Saclay,
F-91191 Gif-sur-Yvette Cedex, France

ABSTRACT

We perform a non-perturbative sum over geometries in a (2+1)-dimensional quantum gravity model given in terms of Causal Dynamical Triangulations. Inspired by the concept of triangulations of product type introduced previously, we impose an additional notion of order on the discrete, causal geometries. This simplifies the combinatorial problem of counting geometries just enough to enable us to calculate the transfer matrix between boundary states labelled by the area of the spatial universe, as well as the corresponding quantum Hamiltonian of the continuum theory. This is the first time in dimension larger than two that a Hamiltonian has been derived from such a model by mainly analytical means, and opens the way for a better understanding of scaling and renormalization issues.

1 Introduction

Trying to come up with *any* method by which the non-perturbative regime of four-dimensional quantum gravity could be probed quantitatively is a challenging task. Given the strongly interacting nature of the problem, one would hope to be able to attack it by a combination of numerical and analytic tools, informing and complementing each other. Starting in two spacetime dimensions [1, 2], a potentially powerful approach to quantum gravity has been developed over the last few years under the name of *Causal Dynamical Triangulations*, or CDT for short. In the grand tradition of *Quantum Regge Calculus* and the program of (non-causal, Euclidean) *Dynamical Triangulations*, its aim is the evaluation of a non-perturbative path integral over spacetime geometries, represented as a state sum over piecewise flat triangulations (see [3, 4, 5] for review material).

Although CDT models for pure gravity can be solved exactly in a variety of ways in (1+1) dimensions [1, 6, 7, 8, 9, 10, 11], it is difficult to extend any of the analytical treatments to the case of higher dimensions, where most of the important results so far have come from numerical simulations [12, 13, 14, 15].[1] An exception to this is the attempt to solve the (2+1)-dimensional CDT model[2] by mapping "thick slices" of its spacetime geometries to configurations of a two-dimensional matrix model with ABAB-interaction [18, 19, 20]. An exact solution of the matrix model relevant to computing the CDT transfer matrix has been given [21, 22], but its rather complicated and implicit form has so far been an obstacle to performing its continuum limit analytically, and thus extracting a quantum Hamiltonian.

This situation is not particularly surprising, as most known solvable statistical models are only one- or two-dimensional. Even a simple spin model like the Ising model has been solved only in two dimensions, and for zero external field. One can therefore already anticipate that an extension of analytical methods and results to the case of higher-dimensional CDT models will be a challenging task. One possible way to approach this problem is to try to modify the model by making simplifying assumptions to improve its solubility, but without changing its physical content in the continuum. The main aim of the present work is to study such a modified model of three-dimensional CDT, which is a particular case of a class of models introduced in [23].[3] Compared with the full CDT model, the ensemble of geometries we will use possesses an additional notion of "order", which will enable us to bring a number of technical tools to bear on its solution. As we will see, this leads to a non-trivial dynamics for the three-dimensional quantum universe, justifying the ansatz retrospectively.

Despite the technical simplification it introduces, the particular three-dimensional CDT model we will be considering is still too complicated to be solved in full generality. In this situation, the special properties of three-dimensional continuum gravity come to our help. Since there are no local, gravitonic field excitations in three dimensions, the dynamical content of this model is encoded in a number of *global* metric variables describing the universe as a whole. One can perform a classical, canonical constraint analysis à la Dirac of (2+1)-dimensional general relativity to see explicitly how the number of degrees of freedom is reduced from infinite to finite (see, for example, [24]).

The way in which we will make use of this property in the non-perturbative path-integral setting of the CDT approach, which works entirely in terms of geometries (that is, on the quotient space of metrics modulo diffeomorphisms), is by integrating over almost all degrees of freedom in the transfer matrix of our model. The resulting "effective" quantum Hamiltonian we are able to derive in the continuum limit will therefore only depend on those degrees of freedom we *anticipate* to be left over as the physically relevant ones. Most importantly, this is the volume (two-dimensional area) of the spatial universe. An extension to include an additional, global Teichmüller parameter may also be technically feasible, but will not be presented here. In the course of the calculation, we find more evidence for a non-perturbative cancellation of the divergent

[1] CDT's precursor of "Dynamical Triangulations" did see some interesting attempts at using analytic tools to understand the model's phase structure in four dimensions, at both strong and weak coupling [16, 17].

[2] More precisely, a version of CDT defined on an extended ensemble of spacetimes allowing for certain "wormhole" degeneracies of the local geometry.

[3] One of the main motivations there was the desire to formulate CDT models with (approximate) spherical symmetry, like those describing a black hole.

conformal mode of the Euclideanized gravitational path integral[4], already evident in other investigations of causal dynamically triangulated models in dimensions three [26] and four [15].

This paper is organized as follows. In Sec. 2 we describe the geometric configurations whose partition function we are going to study and use as a transfer matrix. The configurations are from an ensemble of triangulations of product type, interpolating between successive constant-time slices, with free boundary conditions and boundary cosmological constants, conjugate to the areas of the slices. In Sec. 3 we introduce the first tool that will help us in solving the three-dimensional CDT model, the inversion formula for *heaps of pieces*. In Sec. 4 we reformulate the partition function in terms of the transfer matrices for a set of one-dimensional hard bi-coloured dimer models. In Sec. 5 we study the location of the singularities of the partition function and define a critical surface in the parameter space, which is the boundary of the region where the model is convergent and well defined. In Sec. 6 we introduce the second tool we will need for the solution, the replica trick for products of random matrices. This enables us to identify a critical point on the critical surface where the mean volume goes to infinity, thus making it a potential candidate for taking a non-trivial continuum limit. We can give an exact solution to the model at this critical point, and approximate it to the desired order in the displacement parameter when moving away from it. In Sec. 7 we start exploring the continuum properties of the model by deriving expectation values for the volume and curvature of spacetime. In Sec. 8 we construct the area-to-area transfer matrix by summing over unphysical degrees of freedom, and explain the procedure for extracting information about the spatial volume of the universe. In Sec. 9 we show that for a vanishing bare inverse gravitational constant, one obtains a well-defined quantum Hamiltonian acting on the Hilbert space of the area eigenstates. By contrast, a canonical scaling ansatz for the gravitational constant does not seem to lead to a meaningful result. Finally, our conclusions are presented in Sec. 10. – Four appendices collect various technical results and discussions needed in the main text.

2 Introducing the model

2.1 The product type triangulations

Part of our strategy for trying to solve the non-perturbative three-dimensional model of quantum gravity defined by causal dynamical triangulations (CDT) is to identify a suitable (sub-)class of all CDT configurations whose superposition can be tackled *analytically*. The aim of such a reduction is to simplify the analytic treatment, without eliminating relevant degrees of freedom to such a degree that the universality class is changed, compared to that of the full CDT model.[5] To achieve this, we propose to work with a set of triangulated, causal geometries which have an additional "order" imposed on them. This order is mild in the sense of not implying "isometries" of the triangulations: both the local spacetime curvature and the local curvature of spatial slices can still vary arbitrarily. Our model therefore has less order than the hexagon model considered in [27], which has flat spatial slices.

The way in which we will introduce more structure or order on triangulated spacetimes – inspired by similar earlier ideas [28, 23] – is that of applying the building principle inherent in *causal* dynamical triangulations twice over. This "causality principle" recognizes that in a metric spacetime of Lorentzian signature not all directions are equivalent, but there is a distinguished (class of) time direction(s), in line with the existence of light cones and causal relations, none of which are present in spaces of purely Euclidean signature. In CDT this causal structure is implemented via a discrete global time slicing [2]. This simply means that each simplicial building block of a triangulated spacetime must be contained in exactly one spacetime

[4] Also a continuum treatment in proper-time gauge, which presumably comes closest to the coordinate-free CDT formulation, strongly suggests that the kinetic term for the conformal factor of the spatial geometries (the would-be propagating field degree of freedom) is cancelled in the path integral by a Faddeev-Popov determinant in the measure [25].

[5] This assumes that the full CDT model, which has been studied in Monte Carlo simulations [26], leads to an essentially unique three-dimensional quantum gravity theory. Strictly speaking, rather little is known in dimension three about the universality classes of statistical models of random geometry like the one we are using. There are certainly more, but we are only interested in those which possess a continuum interpretation in terms of quantum gravity.

"sandwich" (the region between discrete proper times t and $t+1$). This implies a causal ordering on the simplices, without constraining the local curvature degrees of freedom.

In addition to this physically motivated choice of a distinguished time direction, which is one of the key ingredients of the approach of causal dynamical triangulations, we will introduce here a second distinguished direction, but this time purely for computational convenience, and under the assumption that it will not affect the universal properties of the gravitational model[6]. This will roughly speaking correspond to an additional slicing, but this time in one of the spatial directions. As explained in [23], the resulting structure can be thought of as a staggered fibration in a piecewise flat setting.

To illustrate the main idea behind this type of triangulation let us start from the easier (1+1)-dimensional CDT model. A spacetime contributing to the sum over geometries is usually described as a sequence of triangulated strips glued together, where each strip represents a piece of spacetime between proper times t and $t+1$, and the lengths of the spatial boundaries of adjacent strips must match pairwise. For our purposes, it is useful to think of a strip as being constructed "sideways" (see Fig.1): starting from a segment (a time-like link), build a frame on it and then fill the frame with some sequence of up- and down-triangles. We will refer to this construction as "building a two-dimensional *tower* over a link". The entire two-dimensional triangulated spacetime can then be regarded as a fibration over a one-dimensional chain of links.

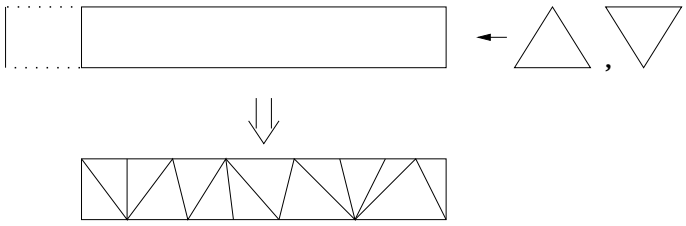

Figure 1: A triangulated strip constructed as a tower over a one-dimensional link.

More generally, *product triangulations* [23] are obtained by building towers over (arrays of) higher-dimensional simplices, such as triangles. How a three-dimensional tower is built over a triangle is illustrated in Fig.2.[7] If the base space is not just a single triangle, but a two-dimensional triangulation consisting of n triangles, we can construct a three-dimensional product triangulation by erecting a tower over each of them, in such a way that the boundary triangulations of the resulting prisms again match pairwise. A general $(n+m)$-dimensional product triangulation is a simplicial manifold constructed by consistently building $(k+m)$-dimensional towers (for all $k \leq n$) over the k-dimensional sub-simplices of an n-dimensional *base* simplicial manifold.

In the present work we will use this construction in the context of (2+1)-dimensional causal dynamical triangulations. By definition, these spacetimes can be regarded as product triangulations whose base space – like in (1+1) dimensions – is a one-dimensional triangulation in the time direction, and the fibres over each link of the base space are the sandwiches between integer values of the discrete time t introduced earlier. Now, instead of allowing sandwich geometries which are arbitrary triangulations of thickness $\Delta t = 1$, we will impose an additional product structure on them. Namely, they should themselves have the form of a sequence of up- and down prisms, as depicted in Fig. 3 below. That is, in addition to the slicing of the entire spacetime corresponding to the global discrete proper time, each sandwich possesses a discrete slicing in a given spatial direction. The number of slices (that is, the number of prisms in a sandwich) is allowed to vary from sandwich to sandwich.

[6] An assumption that obviously will have to be borne out by the final result.

[7] It should be noted that the figures do not represent faithfully the *metric* properties of the building blocks, that is, their edge lengths. By construction, up to a relative factor between space- and time-like links, the edge lengths in a causal dynamical triangulation are all identical.

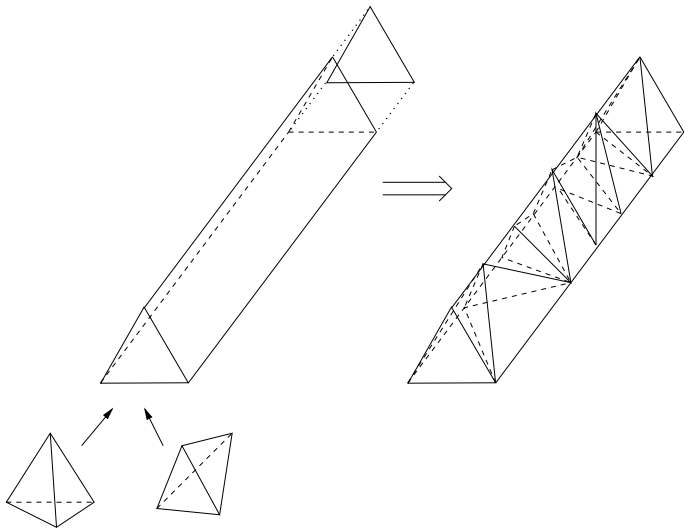

Figure 2: A triangulated prism constructed as a tower over a two-dimensional triangle.

An equivalent way of characterizing such spacetimes is to regard them as fibrations over a two-dimensional base space (with one space- and one time-dimension) which is itself an arbitrary (1+1)-dimensional CDT, and where over each triangle of the base space we have erected a tower "filled" with a sequence of tetrahedra, in such a way that the triangulations on the faces of neighbouring towers match and can be glued together consistently. In this way, we may think of our triangulations as being (1+1+1)-dimensional.

2.2 The partition function

We will concentrate on the dynamics of a "sandwich geometry", given by the transition amplitude from a spatial geometry at time t to one at time $t+1$, in other words, the transfer matrix $\hat{T}$ of the causal dynamical triangulation (CDT) model, which in turn contains information about its quantum Hamiltonian $\hat{H}$ by virtue of the relation $\hat{T} = e^{-a\hat{H}}$ (see [2] for details).

Since pure gravity in (2+1) dimensions does not possess any local, propagating degrees of freedom, we expect that most details of the spatial geometries will be dynamically irrelevant, leaving only the spatial two-volume $A(t)$ and the Teichmüller parameters (together with their canonically conjugate momenta) as physical degrees of freedom. Therefore, rather than calculating the matrix elements

$$G(g_1, g_2, \Delta t = 1) = \langle g_2 | \hat{T} | g_1 \rangle \tag{1}$$

of the transfer matrix from an arbitrary spatial triangulated geometry $|g_1\rangle$ at time t to an arbitrary $|g_2\rangle$ at time $t+1$, we will only keep track of the two boundary areas A_1 and A_2 and evaluate the reduced matrix elements

$$G(A_1, A_2, \Delta t = 1) = \langle A_2 | \hat{T} | A_1 \rangle, \tag{2}$$

where $|A_i\rangle$ is a normalized linear combination of states $|g_i\rangle$ with given area A_i (see [18] for a detailed discussion). Note that one is still summing over the *same* sandwich geometries as in (1), so the reduced matrix elements still capture the effective dynamics of *all* geometric excitations of the sandwich geometry.[8]

[8]The presence of physical degrees of freedom beyond the spatial area depends on the topology of the spatial slices. There are none for the case of spherical slices considered in [26, 18], and there is one Teichmüller parameter in the present model,

Once these matrix elements are known, a next step is to try to extract the continuum Hamiltonian operator $\hat{H}$ of the system from an expansion in the short-distance cutoff a as $a \to 0$ according to

$$\langle A_2|\hat{T}|A_1\rangle = \langle A_2|e^{-a\hat{H}}|A_1\rangle = \langle A_2|\left(\hat{1} - a\hat{H} + O(a^2)\right)|A_1\rangle. \tag{3}$$

We will denote by N_{ij} the number of simplices having i vertices on the initial boundary spatial slice at time t and j on the final one at $t+1$. In this way A_1 (resp. A_2) is given by N_{31} (resp. N_{13}). The prescription for evaluating the discrete one-step propagator (2) is given by

$$G(N_{31}, N_{13}, \Delta t = 1) = \sum_{\mathcal{T}_{|N_{31},N_{13}}} \frac{1}{C_{\mathcal{T}}}\, e^{-S_{EH}}, \tag{4}$$

where the sum is over all sandwich triangulations $\mathcal{T}$ with fixed boundary areas N_{31} and N_{13}, S_{EH} the Wick-rotated discrete Einstein-Hilbert action, and $C_{\mathcal{T}}$ the order of the automorphism group of $\mathcal{T}$. Taking into account boundary terms in the action to ensure the correct propagator behaviour, we find

$$S_{EH} = \alpha(N_{13} + N_{31}) + \beta N_{22} + \gamma N \tag{5}$$

as an explicit expression for the gravitational action, where N is the number of triangle towers in the sandwich, and where we have introduced the parameters

$$\begin{aligned} \alpha &= -c_1 k + b_1 \lambda \\ \beta &= c_2 k + b_2 \lambda \\ \gamma &= c_3 k \end{aligned} \tag{6}$$

depending on the dimensionless bare cosmological and inverse Newton constants λ and k, and on positive numerical constants c_i and b_i characterizing the geometric construction (see appendix A-I).

As one might have anticipated from previous investigations of related three-dimensional quantum gravity models, the evaluation of (4) remains a challenging task, also for our specific choice of ensemble of triangulations. Our main aim will be to calculate its discrete Laplace transform

$$\begin{aligned} Z(x, y, \Delta t = 1) &= \sum_{N_{31}} \sum_{N_{13}} x^{N_{31}} y^{N_{13}} G(N_{31}, N_{13}, \Delta t = 1) \\ &= \sum_{N_{31}} \sum_{N_{13}} (xe^{-\alpha})^{N_{31}} (ye^{-\alpha})^{N_{13}} \sum_{\mathcal{T}_{|N_{13},N_{31}}} e^{-\beta N_{22} - \gamma N} \\ &= \sum_{\mathcal{T}} u^{\frac{N_{31}}{2}} v^{\frac{N_{13}}{2}} w^{N_{22}} e^{-\gamma N}, \end{aligned} \tag{7}$$

where the sum runs over all triangulations $\mathcal{T}$ compatible with the structure discussed above, and we have introduced the weights $\sqrt{u} = xe^{-\alpha}$, $\sqrt{v} = ye^{-\alpha}$ and $w = e^{-\beta}$. In writing (7), we have set $C_{\mathcal{T}}$ equal to one, because for the chosen boundary conditions its contribution in the continuum limit will be negligible. The function $Z(x, y, \Delta t = 1)$ can be thought of either as the generating function of $G(N_{31}, N_{13}, \Delta t = 1)$, or as the partition function of the sandwich geometry with free boundary conditions (thus summing over all values of the boundary volume) and with additional weights $x = e^{-\lambda_{in}}$ and $y = e^{-\lambda_{out}}$, corresponding to additional boundary cosmological terms in the action.

To get back the transfer matrix from $Z(x, y, \Delta t = 1)$, one needs to keep x and y distinct and variable. However, as shown by other examples (see the end of section 3.1 for the two-dimensional case, and [26] for a numerical illustration in three dimensions), one may be able to extract non-trivial information about the

where we choose boundary conditions corresponding to cylindrical spatial slices [29]. Work is under way to determine whether the calculation of matrix elements presented here is still feasible when the dependence on this parameter is kept explicitly.

phase structure of the model by considering the special values $x = y = 1$, which simplifies the evaluation of (7).

At this stage we will exploit the special product structure of our chosen spacetime geometries to split the sum over all sandwich triangulations into two simpler sums. The idea is to first perform the sum over all fillings (i.e. triangulations) of towers for a *fixed* triangulated base strip, and then to perform the sum over all possible triangulations of the base strip (see Fig.3), schematically

$$\sum_{\mathcal{T}_{sandwich}} = \sum_{\mathcal{T}_{base\ strip}} \sum_{\mathcal{T}_{towers}} . \tag{8}$$

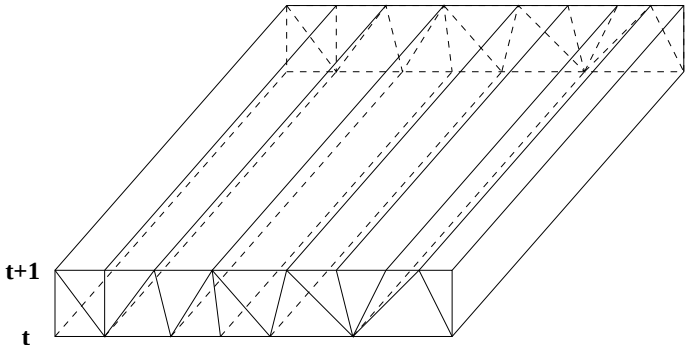

Figure 3: A "sandwich geometry" of product type in the (1+1+1)-dimensional CDT model, built over a given triangulated base strip. We split the calculation of its partition function into two parts, calculating first the partition function for such a geometry and then summing over all possible sequences of towers. By "towers of type (2,1)" we will mean the towers built on a triangle with two vertices at time t and one at time $t+1$, and similarly for "towers of type (1,2)". Each of the towers is filled up with a sequence of tetrahedra, as illustrated in Fig. 2. There are three different possibilities for how a tetrahedron can be oriented inside one of the prisms (see [23] for more geometric details). The apparent "straightness" of the towers is again an artefact of our representation, which emphasizes the product structure.

We are thus naturally led to studying the partition function Z_N for sandwich geometries of product type with N towers, and investigating its properties in the large-N limit. In this sense we are treating the second distinguished direction, which defines the slicing within the sandwich geometry, in the same way as we treat the time direction in (1+1)-dimensional CDT. It is related to (7) via

$$Z(x, y, \Delta t = 1) = \sum_N e^{-\gamma N} Z_N(u, v, w), \tag{9}$$

with Z_N expressible as

$$Z_N(u, v, w) = \sum_{S_N} Z_{S_N}(u, v, w) = \sum_{S_N} \sum_{\mathcal{T}_{S_N}} u^{\frac{N_{31}}{2}} v^{\frac{N_{13}}{2}} w^{N_{22}}, \tag{10}$$

where the sequences S_N consist of N prism towers, $N - R$ of them of type (2,1) and R of type (1,2), for any $R < N$.

3 Inversion formula

The special product form of our sandwich geometries will enable us to make use of an *inversion formula*, relating its partition function to that of a model of one dimension less. As we will review in the next

subsection, this technique essentially provides a complete solution to the CDT model in dimension (1+1). This is not true in the much more involved case of CDT in dimension (1+1+1) we are addressing here, but – as we will demonstrate – it will nevertheless allow us to make substantial progress in the evaluation of the partition function.

3.1 The two-dimensional case

The partition function of the full (1+1)-dimensional CDT model [1], more specifically, the partition function of its equivalent dual formulation in terms of three-valent graphs [7], can be expressed as the inverse of the partition function Z^{hd} of a hard-dimer model in *one* dimension [28], namely,

$$Z_t^{2d}(u=g^2) = \frac{1}{Z_t^{hd}(-u)}, \tag{11}$$

where

$$Z_t^{hd}(u) = \sum_{\text{hard dimer config. } D} u^{|D|}, \tag{12}$$

$g = e^{-\lambda}$ is the volume weight assigned to each triangle and t is the number of time steps. We recall the proof of this inversion formula in appendix A-II.

This is not an isolated result, but can be seen as a particular instance of a more general mathematical result which can already be found in earlier work [30], where also the notion of a *heap of pieces* was introduced. Roughly speaking, a heap of pieces is a partially ordered set whose elements occupy columns out of a finite set of columns, and where direct-order relations only exist between elements in the same column or in neighbouring ones. It is not difficult to realize that triangulations of product type are closely related to the heap-of-pieces construction, and in particular that the structure of the (1+1)-dimensional CDT model (in its dual picture) is that of a heap of dimers.

One can also re-express the partition function (12) in a transfer matrix formulation. This is done by introducing a two-dimensional vector space associated to each site, with the vector $(1,0)$ corresponding to the empty state, and $(0,1)$ to an occupied dimer state at the site. If we attach a weight 1 to the transition empty-empty (between neighbouring dimers), a weight $\sqrt{u}$ to the transition dimer-empty or empty-dimer, and a weight 0 to the transition dimer-dimer, we obtain a transfer matrix M associated with such a transition. Since the dimer partition function for the case of periodic boundary conditions is given by $\mathrm{Tr}\,(M^t)$, we can rewrite (11) as

$$Z_t^{2d}(u=g^2) = \frac{1}{\mathrm{Tr}\begin{pmatrix} 1 & \mathrm{i}\sqrt{u} \\ \mathrm{i}\sqrt{u} & 0 \end{pmatrix}^t}. \tag{13}$$

Since $\mathrm{Tr}\,(M^t) = \lambda_+^t + \lambda_-^t$, where $\lambda_\pm = (1 \pm \sqrt{1-4u})/2$ are the two eigenvalues of the transfer matrix, we have

$$Z_t^{2d}(u=g^2) \sim \frac{1}{\lambda_+(u)^t} \tag{14}$$

for large t, which is non-analytical in $u = 1/4$, the critical point.

Alternatively, this critical point can already be found by analyzing the one-step propagator

$$Z_{t=1}^{2d}(i,j|g) = \sum_{strips\ \mathcal{T}_{|i,j}} \frac{1}{C_{\mathcal{T}}} e^{-S_{EH}} \tag{15}$$

of the (1+1)-dimensional model, given by a sum over triangulated strips $\mathcal{T}_{i,j}$ with an initial boundary of length i and a final boundary of length j. Since the Einstein-Hilbert action consists only of the volume term (multiplied by the cosmological constant λ), the propagator (15) reduces to

$$Z_{t=1}^{2d}(i,j|g=e^{-\lambda}) = e^{-\lambda(i+j)} \sum_{strips\ \mathcal{T}_{|i,j}} 1 \tag{16}$$

with the corresponding generating function

$$Z^{2d}_{t=1}(x,y|g=e^{-\lambda}) = \sum_{i,j\geq 0} x^i y^j e^{-\lambda(i+j)} \sum_{strips\ \mathcal{T}_{|i,j}} 1. \tag{17}$$

With the help of the inversion formula (and considering x and y as the square roots of the weights of the boundary dimers), the latter can now be rewritten as

$$Z^{2d}_{t=1}(x,y|u=e^{-2\lambda}) = \frac{1}{\begin{pmatrix}1 & \mathrm{i}y\end{pmatrix}\begin{pmatrix}1 & \mathrm{i}\sqrt{u}\\ \mathrm{i}\sqrt{u} & 0\end{pmatrix}\begin{pmatrix}1\\ \mathrm{i}x\end{pmatrix}} = \frac{1}{1-\sqrt{u}(x+y)}. \tag{18}$$

We observe that by setting $x=y=1$ (*i.e.* considering the partition function for $\Delta t=1$ with free boundary conditions), we get a singularity in the point $\sqrt{u}=\frac{1}{2}$. This is exactly the critical point, and the continuum limit has to be taken by fine-tuning λ to its critical value $\lambda_c=\ln 2$. It is straightforward to see that in this limit $\langle V\rangle = -\frac{1}{Z}\frac{\partial Z}{\partial \lambda}$ diverges, as required. Of course, the full one-step propagator (18) with $x\neq y$ contains much more information; indeed, as demonstrated in [1], one can recover from it the quantum Hamiltonian of the model in the continuum limit.

3.2 The three-dimensional case

In order to apply the inversion formula to the case of three-dimensional causal triangulations, we will use the fact that the propagator of this model can be characterized in terms of geometric data which are "almost" two-dimensional, an observation already underlying earlier investigations of three-dimensional CDT in terms of the ABAB-matrix model [18, 19, 20]. The argument runs as follows. Consider a three-dimensional sandwich geometry, made up of a single layer of tetrahedra glued together pairwise along their time-like triangular faces. For a given tetrahedron, there are three possibilities for its orientation relative to the initial slice at time t and the final slice at time $t+1$, characterized again by the numbers (i,j) of vertices it shares with either slice.

Now take a two-dimensional spatial slice through the sandwich geometry at time $t+1/2$. This is a well-defined prescription since the discrete time t can be continued uniquely inside the simplices by virtue of their flatness [23]. The surface at $t+1/2$ is piecewise flat, consisting of flat triangles (coming from tetrahedra of type (3,1) and (1,3)) and flat squares (from the tetrahedra of type (2,2)), see Fig. 4.[9] However, it is clear that given this triangulation alone, we cannot reconstruct the original three-dimensional sandwich geometry. For this we need to know whether a given triangle at $t+1/2$ came from a (3,1)- or a (1,3)-tetrahedron, or, equivalently, whether a given link of the triangulation came from a time-like (2,1)- or (1,2)-triangle. One way to keep track of this information is to colour-code the two types of links, as shown in Fig. 4. By saying that the one-step propagator cannot be characterized by two-dimensional geometric data alone, we meant the need for this additional colouring information.

In order to map the partition function for the bi-coloured two-dimensional geometries to that of a hard-dimer model, we first go to the bi-coloured graphs dual to the triangulations. The links of the dual graphs are obtained by connecting the centres of neighbouring triangles and squares, and their colour is inherited from the colour of the crossing link of the original triangulation (see Fig. 5).

As a consequence of the product structure for the sandwich geometries, also the dual graphs obtained in this way have a special form. Namely, part of the dual graph can be drawn as a fixed sequence of straight lines (which we will call "vertical lines", and which are drawn vertically in Fig. 6) coming from the prism towers, blue for a tower over a type-(2,1) triangle and red for a tower over a type-(1,2) triangle. The sequence of blue and red towers depends on the triangulation of the base strip. In addition, the dual graph contains "horizontal links", which start on a vertical line of the same colour and end on the next (to the right, say) vertical line of the same colour. The position of the horizontal links encodes the three-dimensional triangulation of the original sandwich geometries.

[9] By a slight abuse of language, we will keep referring to this geometry as a "triangulation".

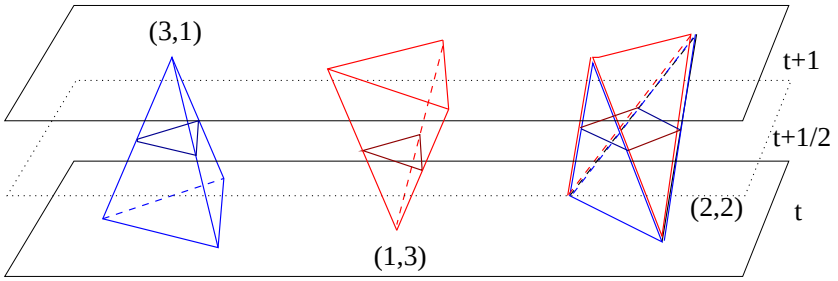

Figure 4: The three types of tetrahedral building blocks and their intersections at time $t + 1/2$.

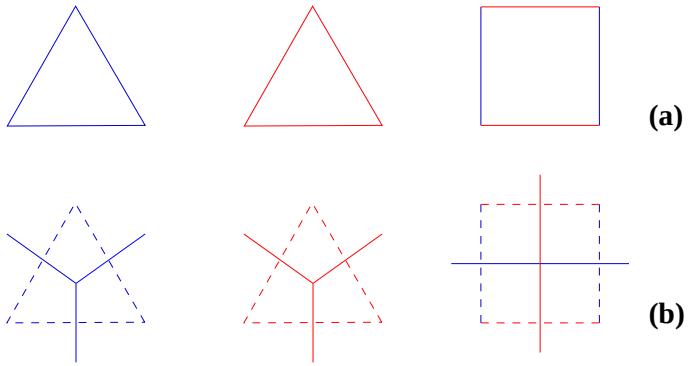

Figure 5: The elementary building blocks of the coloured "triangulation" at time $t + 1/2$ characterizing a sandwich geometry (a), together with their duals (b).

Looking at the subgraphs of one colour in the dual graph example of Fig. 6, one notes that they are particular examples of dual graphs for (1+1)-dimensional CDT spacetimes. It is indeed the case that the blue graph is precisely the graph dual to the triangulation of the initial two-dimensional surface of the sandwich geometry, and the red graph the dual to its final surface. We may therefore think of the bi-coloured graph as a particular superposition of these two uni-coloured graphs. Bi-coloured graphs of this type are again of the form of *heaps of pieces* in the sense of [30], which means that we can map them to dimer configurations as in the (1+1)-dimensional situation above (c.f. appendix A-II), but with the difference that now the one-dimensional dimer model will also be bi-coloured, with a fixed sequence of blue and red sites and with the blue (red) dimers linking a blue (red) site with the next one of the same colour, as depicted in Fig. 6.

The upshot of our considerations so far is that for a sandwich geometry associated with a fixed triangulation S_N of the base strip an analogue of formula (11) holds, namely,

$$Z_{S_N}(u, v, w) = \frac{1}{Z^{hcd}_{S_N}(-u, -v, w)}, \tag{19}$$

where

$$Z^{hcd}_{S_N}(u, v, w) = \sum_{\text{coloured hard}-\text{dimer config. } D_{|S_N}} u^{|D|_b} v^{|D|_r} w^{|\cap D|} \tag{20}$$

is the partition function of the coloured dimer problem for a given sequence S_N of blue and red sites, $|D|_b$

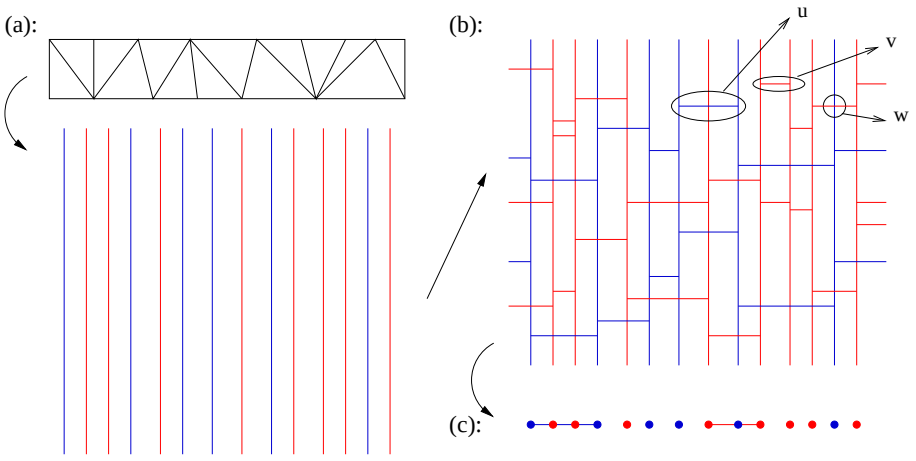

Figure 6: From sandwich geometries with product structure to hard dimers: (a) vertical lines representing towers over a triangulated base strip; (b) horizontal links encode how the tetrahedra are connected, the corresponding weights can be read off as indicated; (c) projection to a sequence of hard-dimer configurations, as explained in appendix A-II.

($|D|_r$) is the number of blue (red) dimers in the configuration D, and $|\cap D|$ is the number of crossings between dimers and sites of different colour. We should emphasize that our application of the inversion formula relates only to the *second* sum in (8), since we sum over the triangulation of the towers for a *fixed* triangulation of the base strip. This allows us to rewrite (9) as

$$Z(x,y,\Delta t=1)=\sum_N e^{-\gamma N} Z_N(u,v,w)=\sum_N e^{-\gamma N}\sum_{S_N}\frac{1}{Z^{hcd}_{S_N}(-u,-v,w)}, \tag{21}$$

whose further evaluation will be the subject of the remainder of the paper.

4 Random matrix formulation

The coloured-dimer partition function can be written in terms of transfer matrices, by introducing three vectors (1,0,0), (0,1,0) and (0,0,1) corresponding to an empty link, a blue link and a red link between neighbouring sites. A transfer matrix can be associated with transitions between these states, taking into account that hard dimers are not allowed to touch each other, and that a dimer of a given colour connects only sites of the same colour which are first neighbours (among the sites with same colour), and may cross sites of the opposite colour in between. The transfer matrices can therefore be associated with the sites or vertices of the dimer model, and their explicit form depends on the colour label of the site. The transition empty-empty gets a weight 1, the transitions dimer-empty or empty-dimer get a weight $\sqrt{u}$ or $\sqrt{v}$, depending on the colour, and the crossing of a site by a dimer of any colour gets a weight w; all other possibilities have weight 0. In this way we can associate a matrix

$$\tilde{A}=\begin{pmatrix}1 & \sqrt{u} & 0\\ \sqrt{u} & 0 & 0\\ 0 & 0 & w\end{pmatrix} \tag{22}$$

with every blue site, and a matrix

$$\tilde{B}=\begin{pmatrix}1 & 0 & \sqrt{v}\\ 0 & w & 0\\ \sqrt{v} & 0 & 0\end{pmatrix} \tag{23}$$

with every red site. Consequently, the partition function $Z^{hcd}_{S_N}(u,v,w)$ can be expressed as a product of N matrices $\tilde{A}$ and $\tilde{B}$, ordered according to the sequence specified by S_N (note that the matrices $\tilde{A}$ and $\tilde{B}$ do not commute). We can now write the partition function (19) associated with a fixed sequence S_N as[10]

$$Z_{S_N}(u,v,w) = \frac{1}{\mathrm{Tr}\,(ABAABABBB...)_{S_N}} \tag{24}$$

where the matrices A and B are the same as $\tilde{A}$ and $\tilde{B}$, but with the substitution $\sqrt{u} \to \mathrm{i}\sqrt{u}$, $\sqrt{v} \to \mathrm{i}\sqrt{v}$. In order to express the sum over sequences S_N in eq. (10), it is convenient to combine the two matrices and define a general transfer matrix

$$M_{q_j}(u,v,w) = q_j A + (1-q_j)B = \begin{pmatrix} 1 & q_j \mathrm{i}\sqrt{u} & (1-q_j)\mathrm{i}\sqrt{v} \\ q_j \mathrm{i}\sqrt{u} & (1-q_j)w & 0 \\ (1-q_j)\mathrm{i}\sqrt{v} & 0 & q_j w \end{pmatrix}, \tag{25}$$

with q_j taking the values 1 ($M = A$) or 0 ($M = B$). The sum over sequences S_N is then replaced by a sum over sequences in $\{0,1\}^N$. In this formulation, the calculation of the partition function assumes the form of a problem of products of random matrices [31], and we can rewrite the full partition function (9) as

$$Z(x,y,\Delta t=1) = \sum_N e^{-\gamma N} \sum_{\{q_j\}_N} \frac{1}{\mathrm{Tr}\,\prod_{j=1}^N M_{q_j}(u,v,w)}. \tag{26}$$

This in turn can be thought of as the average of (24) over all possible configurations $\{q_j\}_N$, with $q_j = 1$ and $q_j = 0$ each having probability $p = 1/2$. Introducing the notation

$$|P_{N,\{q\}}(u,v,w)| = \mathrm{Tr}\,\prod_{j=1}^N M_{q_j}(u,v,w), \tag{27}$$

we can finally write

$$Z(x,y,\Delta t=1) = \sum_N e^{-\gamma N} Z_N(u,v,w) = \sum_N (2e^{-\gamma})^N \left\langle \frac{1}{|P_{N,\{q\}}(u,v,w)|} \right\rangle, \tag{28}$$

where we have used the normalized ensemble average $\langle \bullet \rangle \equiv 2^{-N} \sum_{\{q_j\}} \bullet$.

5 The zeros of the denominators

An important feature to be noted about the inversion formula is that it maps an infinite series with positive coefficients to the inverse of a finite sum with alternating sign coefficients. The latter will have a real root corresponding to the radius of convergence of the infinite series. This is evident in the (1+1)-dimensional case, formula (18). The same is clearly true for the (1+1+1)-dimensional case (19) too, which will have a two-dimensional *locus* of zeros in the three-dimensional parameter space spanned by u, v and w. However, the location of this locus will depend on the sequence $\{q_j\}$, and we must keep in mind that we still have to sum over all the sequences $\{q_j\}$. Consequently, we will be interested in determining the envelope of all the loci. In the absence of an analytical solution, which appears difficult to come by, we will determine its location in the limit of infinite N by studying particular classes of sequences and by numerical computations, in conjunction with a bit of (well-motivated) conjecture.

[10] Our choice of taking the trace in the denominator implies periodic boundary conditions in one of the spatial directions, by gluing together the first and last prism tower of the sandwich. Since we are leaving the other spatial direction open, the spatial slices of our model have the topology of a cylinder. Instead of compactifying one of the directions, we could also have left it open, in which case we would have to specify the boundary lengths as boundary conditions, or introduce conjugate boundary variables analogous to the x- and y-variables in (1+1) dimensions, eqs. (17) and (18), and contract the product of matrices with the vectors $(1\ ix_1\ ix_2)$ and $(1\ iy_1\ iy_2)$. This would complicate the treatment of the partition function considerably.

5.1 u = v

Let us temporarily assume that $x = y$ (and eventually $= 1$) in the Laplace transform of the one-step propagator, (7), and therefore $u = v$. This clearly makes things easier, but should still permit us to extract information about the phase structure of the model, as is the case in both two and three dimensions (see [18] and [19] for illustrations of the latter). This is not an implausible proposition in the sense that we want to find the critical line in the k-λ plane, which concerns the "bulk" behaviour of the spacetime and should be insensitive to details of the boundary data, like those encoded in x and y.

In order to determine the zeros of the polynomials $|P_N(u, v = u, w)| = \mathrm{Tr} \prod_{j=1}^{N} M_{q_j}(u, v = u, w)$, we write this product as $A^{n_1} B^{n_2} ... A^{n_{M-1}} B^{n_M}$ for some sequence of $M \leq N$ positive integers $\{n_1, ..., n_M\}$ which sum up to N, $\sum_{i=1}^{M} n_i = N$. Note that from $u = v$ follows $B = JAJ$, where the matrix

$$J = \begin{pmatrix} 1 & 0 & 0 \\ 0 & 0 & 1 \\ 0 & 1 & 0 \end{pmatrix} \tag{29}$$

is a projector (*i.e.* $J^2 = Id$), so that we can write

$$|P_{N,\{q\}}| = \mathrm{Tr}\,(A^{n_1} J A^{n_2} J ... A^{n_{M-1}} J A^{n_M} J). \tag{30}$$

Note furthermore that

$$A^n = \begin{pmatrix} (\alpha^n)_{11} & (\alpha^n)_{12} & 0 \\ (\alpha^n)_{12} & (\alpha^n)_{22} & 0 \\ 0 & 0 & w^n \end{pmatrix}, \tag{31}$$

where α^n is the n-th power of the matrix

$$\alpha := \begin{pmatrix} 1 & \mathrm{i}\sqrt{u} \\ \mathrm{i}\sqrt{u} & 0 \end{pmatrix} \tag{32}$$

found in (13) above, and which has the following properties:

$$(\alpha^n)_{11} = \frac{\lambda_+^{n+1} - \lambda_-^{n+1}}{\lambda_+ - \lambda_-} = u^{\frac{n}{2}} U_n(\frac{1}{2\sqrt{u}}) \tag{33}$$

$$(\alpha^n)_{12} = i\sqrt{u}(\alpha^{n-1})_{11} \tag{34}$$

$$(\alpha^n)_{22} = (\alpha^n)_{11} - (\alpha^{n-1})_{11} \tag{35}$$

where $\lambda_\pm = (1 \pm \sqrt{1 - 4u})/2$ are the eigenvalues of the matrix α (w is the third eigenvalue of the matrix A), and $U_n(x)$ is the n-th Chebyshev polynomial of the second kind.

5.1.1 u=0

For the subcase $u = 0$ everything is trivial since $|P_N(0, 0, w)| = 1$ for every sequence. (We exclude degenerate sequences with N matrices of one type and none of the other, which would yield $|P_N(0, 0, w)| = 1 + w^N$. At any rate, they would give a negligible contribution in the average.) We thus have $Z_N(0, w) = 1$.

5.1.2 w=0

For the subcase $w = 0$ the trace (30) reduces to

$$|P_{N,\{q\}}| = z_0 = \prod_{i=1}^{M} (\alpha^{n_i})_{11} \equiv \prod_{i=1}^{M} u^{\frac{n_i}{2}} U_{n_i}(\frac{1}{2\sqrt{u}}) \tag{36}$$

by virtue of (33), which implies that (30) becomes the product of M uncoupled partition functions of the simple (uncoloured) hard-dimer problem.

Note first of all that the term $u^{\frac{n}{2}}$ in (33) does not vanish at $u = 0$, because its product with $U_n(\frac{1}{2\sqrt{u}})$ gives a polynomial of order $[\frac{n}{2}]$ in u whose zeroth order term is 1. From mathematical handbooks we know that $U_n(x)$ has zeros only in the interval $[-1, 1]$, more precisely, at the values $x_i = \cos(\frac{i}{n+1}\pi)$, for $i = 1, ..., n$. It follows that no zeros can occur for $u < 1/4$. By contrast, for fixed $u > 1/4$ there is always a sequence, for some N, such that $|P_{N,\{q\}}|$ has zeros between $1/4$ and u. For positive $\epsilon = u - \frac{1}{4}$, the occurrence of the first root is when $\frac{1}{2\sqrt{\frac{1}{4}+\epsilon}} \leq x_1 = \cos(\frac{1}{n+1}\pi)$. For small ϵ this requires a large n. And this in turn means that (some but not necessarily all of) the sequences contributing to the critical behaviour at $w = 0$ and $u = \frac{1}{4}$ possess a large group of consecutive matrices of the same kind; particular examples of this are configurations like AB^{N-1}. A predominance of such configurations would signal a decoupling of neighbouring slices in the three-dimensional geometry, and a geometric degeneracy of the model there.

5.1.3 u,w≠0

For both u and w different from zero the general expression for (30) becomes highly non-trivial. To get a better idea of the distribution of zeros, we used the program MATLAB to plot some of the roots of $|P_N(u, w)|$. This is in principle straightforward, but for increasing N requires considerable computing power, because the number of sequences grows like 2^N. A superposition of several such plots is shown in Fig. 7a.[11] From this picture it appears that the singularity-free region for $u < 1/4$ found for $w = 0$ is also present for $w > 0$, up to some value of about 0.5, and then starts to shrink toward zero. Because of the limit on N in our numerical study, we could not determine whether the value $u = 0$ is reached at $w = 1$ or rather some small $u = \epsilon > 0$.

What we can do analytically to put more stringent bounds on the envelope is to study specific sequences and find their locus of zeros asymptotically for $N \to \infty$. We find that $(u, w) = (\frac{1}{4}, w)$ continues to be an accumulation point for the zeros of the sequences AB^{N-1} for all values of $w \leq 1$. For sequences of the form $A^{\frac{N}{2}}B^{\frac{N}{2}}$ it can easily be shown analytically that a solution of $Tr(A^{\frac{N}{2}}B^{\frac{N}{2}}) = 0$ for $N \to \infty$ is given by $w = \lambda_+(u) = (1 + \sqrt{1 - 4u})/2$. For the alternating sequences $(AB)^{N/2}$ we find instead a locus given by $uw = 4/27$, which is tangent to the curve $w = \lambda_+(u)$ in the point $(u, w) = (2/9, 2/3)$, and otherwise lies completely to the right of it (in a u-w-plot like that of Fig. 7a). Many other sequences with regular distribution patterns for A- and B-matrices whose large-N limit we have studied seem to have an asymptotic locus of zeros which is a smooth curve lying in between $w = \lambda_+(u)$ and $w = 4/(27u)$, and passing through their common point $(2/9, 2/3)$.

Based on these findings, and in the absence of any evidence to the contrary, we conjecture that the (u, w)-region free of singularities is defined by the simultaneous conditions $u < 1/4$ and $w < \lambda_+(u)$, whose boundary is given by the red curve in Fig. 7a. To its right we have plotted the locations of zeros, both of random sequences corresponding to some q_i's, and of special sequences we have been able to treat exactly. Interestingly, this singular curve can be characterized in terms of the eigenvalues $(\lambda_+,\ \lambda_-,\ w)$ of the matrix A, as the curve along which the largest two of the eigenvalues are degenerate. For $u > 1/4$, the $\lambda_\pm$ are distinct and complex, and thus cannot be equal to w (which is real). For $u = 1/4$, $\lambda_\pm$ are both equal to $1/2$ and larger than w, as long as $w < 1/2$. For $w \geq 1/2$, the two largest eigenvalues are exactly defined by w being equal to the larger one of the pair $\lambda_\pm$. This suggests the existence of an analytical argument for why such a degeneracy gives rise to roots of $|P_N|$, but we have not been able to find it.

Following this line of argument further, we can give yet another characterization of the singular line. It can be checked that the trace $|P_N|$ is always real. Denoting the eigenvalues of P_N by λ_i, $i = 1, 2, 3$, their sum must therefore be real. Their product is the determinant of P_N, which from (30) is easily computed as the product of the determinants, $\lambda_1\lambda_2\lambda_3 = \lambda_+^N\lambda_-^N w^N = (uw)^N$, which is always real and positive for $u, w > 0$. This leaves only three possibilities for the signature/character of the λ_i: $(+++)$, $(+--)$ or $(+\ c\ \bar{c})$, where

[11] Typical N-values for the sequences ranged between 50 and 200, and the total number of sequences analyzed was on the order of 50.

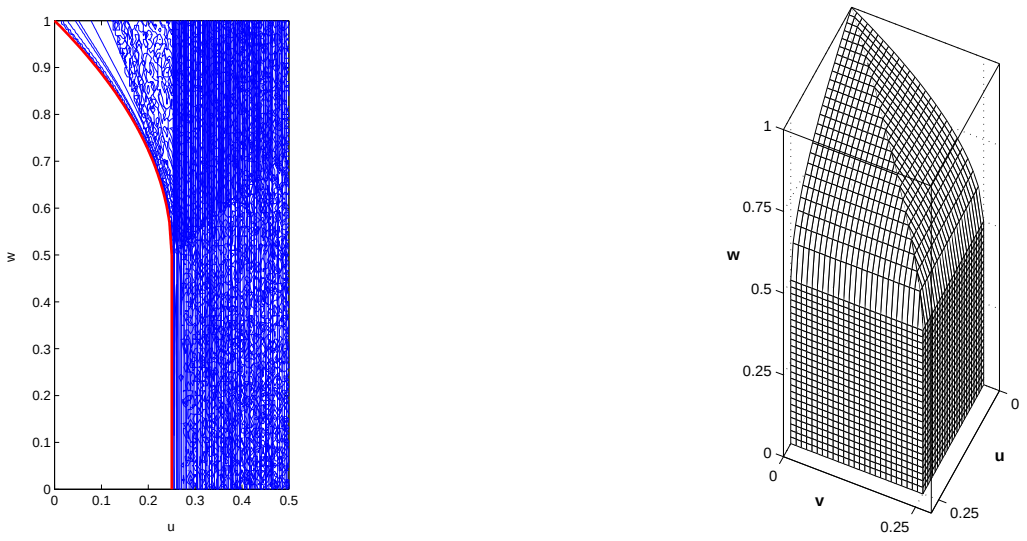

(a) **(b)**

Figure 7: **(a):** The critical line, combined from $u = 1/4$, $w = \lambda_+(u)$, together with plots of the zeros of $|P_{N,\{q\}}|$ for random sequences $\{q\}$ and for sequences AB^{N-1} and $A^{\frac{N}{2}}B^{\frac{N}{2}}$ at different values of N, in the $u = v$ plane. **(b):** The plot of the critical surface in the full parameter space of the (u, v, w).

c and $\bar{c}$ denotes complex conjugates. Of course with signature $(+++)$ the trace can never be zero, and this is precisely the case in the region $u < 1/4$ and $w < \lambda_+(u)$. From this we cannot go directly to signature $(+--)$ because two of the eigenvalues would have to pass through zero, in which case the determinant would become zero, leading to a contradiction. The transition occurring at the singular line should be to the region with $(+\ c\ \bar{c})$. From there, once two of the eigenvalues are complex, their real part can become negative and also the trace can become zero. This scenario is confirmed by numerical computations, but a general, algebraic proof is at this stage still missing.

5.2 $\mathbf{u \neq v}$

Using the same mixture of analytical and numerical methods as for the case $u = v$, and with a comparable computational effort[12] we have found a similar picture in the full three-dimensional parameter space with $u \neq v$. The critical surface is determined by the same relations as for $u = v$ above, but with u substituted by $\max(u, v)$. That is, for $u < v$ the critical surface is given by $v = 1/4$ for $w \leq 1/2$ and $w = \lambda_+(v)$ for $w > 1/2$, while for $u > v$ it is given by $u = 1/4$ for $w \leq 1/2$ and $w = \lambda_+(u)$ for $w > 1/2$. Since our extensive numerical and analytical checks have turned up no contradictions to this picture, we will in the following assume it to be correct. The critical surface is depicted in Fig. 7b.

6 The large-N limit

We will now assume that we are inside the region free of singularities. In this region the partition sum is convergent and its large-N limit well defined. The boundary of this region is the critical line (or critical surface

[12] Amongst other things, by systematically "scanning" the three-dimensional coupling space in (v, w)-planes for various fixed values of u.

for $u \neq v$). We want to characterize the (non-)analytic character of the partition function $Z_N(u,v,w)$ on this boundary *after* the limit for large N has been taken (see the discussion in the previous section). Initially the evaluation of this function seems an insurmountable task, because according to (21) and (26) we have to sum over the *inverses* of the matrix traces resulting from the application of the inversion formula. However, it was exactly with this difficulty in mind that we introduced the reformulation of the partition function in terms of random matrix products in Sec. 4 above. Techniques available for such products of random matrices will help us to estimate precisely the limit we are interested in, namely

$$L_{-1}(u,v,w) = \lim_{N\to\infty} \frac{1}{N} \ln \left\langle \frac{1}{|P_N(u,v,w)|} \right\rangle = -\ln 2 + \lim_{N\to\infty} \frac{1}{N} \ln Z_N(u,v,w,\Delta t = 1), \tag{37}$$

where, as in (28) above, the average has been taken over all random sequences $\{q_j\}$. (The reason for the notation L_{-1} will become clear soon.) The aim of this section is to compute $L_{-1}(u,v,w)$, at least in a perturbative expansion around the critical point (which still needs to be identified).

6.1 Generalized Lyapunov exponents

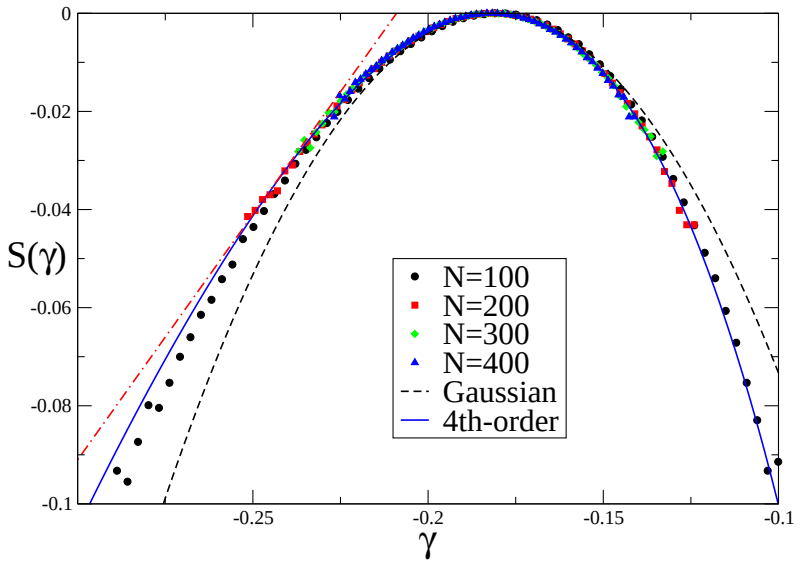

Figure 8: Determining the function $S(\gamma)$ numerically for $u = v = 0.24$ and $w = 0.1$. The Gaussian approximation is shown as a dashed line. The blue continuous line is a fourth-order fit. The straight (dashed-dotted) line on the left has slope 1, and is tangent to $S(\gamma)$ in γ^*_{-1}. In this case, the Gaussian approximation is not sufficient to compute L_{-1} from (44), because in the point $\gamma = \gamma^*_{-1}$, $S(\gamma)$ is very different from the Gaussian fit. The figure illustrates a "worst-case scenario" in that for the chosen parameter values the deviation of the actual curve from the Gaussian approximation is maximal, see also Fig. 9. See appendix A-III for details on the numerical method.

For a given sequence $\{q_j\}$, define a real number γ by

$$\gamma = \frac{1}{N} \ln |P_N|, \tag{38}$$

where $|P_N|$ is a shorthand notation for $|P_{N,\{q\}}(u,v,w)|$. Since $\{q_j\}$ is random, γ will be a random variable as well; its probability distribution has, for large N, the general form [31]

$$\pi_N(\gamma) \propto e^{NS(\gamma)}. \tag{39}$$

The function $S(\gamma)$ is called *large deviations function*; it is a convex function that has a maximum in $\gamma = \bar{\gamma}$, where $\bar{\gamma}$ is defined as

$$\bar{\gamma} = \lim_{N\to\infty} \frac{1}{N} \ln |P_N| \tag{40}$$

and called the *maximum Lyapunov characteristic exponent*.[13] We will choose $S(\bar{\gamma}) = 0$, so that the distribution $\pi_N(\gamma)$ is normalized at the leading order for $N \to \infty$:

$$\int d\gamma\, e^{NS(\gamma)} \sim e^{NS(\bar{\gamma})} = 1. \tag{41}$$

We can then write

$$\left\langle \frac{1}{|P_N(u,v,w)|} \right\rangle = \langle e^{-N\gamma} \rangle = \int d\gamma\, e^{N[S(\gamma)-\gamma]} \sim e^{N[S(\gamma^*)-\gamma^*]}, \tag{42}$$

where γ^* is the solution to the saddle point equation[14]

$$\frac{\partial S(\gamma)}{\partial \gamma} = 1. \tag{43}$$

Similarly, one can define the Legendre transform of $S(\gamma)$ (or *generalized Lyapunov exponent*) by

$$L_n = \lim_{N\to\infty} \frac{1}{N} \ln \langle |P_N|^n \rangle = \lim_{N\to\infty} \frac{1}{N} \ln \langle e^{n\gamma N} \rangle = S(\gamma_n^*) + n\gamma_n^*, \tag{44}$$

where γ_n^* is the solution of

$$\frac{dS}{d\gamma} = -n. \tag{45}$$

Clearly, for integer n, $e^{NL_n} = \langle |P_N|^n \rangle$ is the n-th moment of $|P_N|$. If one approximates $S(\gamma)$ by a Gaussian[15], $S(\gamma) = -\frac{(\gamma-\bar{\gamma})^2}{2\sigma^2}$, one easily finds

$$\gamma_n^* = \bar{\gamma} + n\sigma^2, \qquad L_n = n\bar{\gamma} + \frac{1}{2} n^2 \sigma^2. \tag{46}$$

In this case the knowledge of the first two moments L_1 and L_2 is equivalent to the knowledge of $\bar{\gamma}$ and σ, and determines the full curve L_n, now regarded as an analytic function for all values of n. If $S(\gamma)$ is not exactly Gaussian, a systematic expansion of L_n in powers of n,

$$L_n = \sum_{k=1}^{\infty} \frac{l_k}{k!} n^k, \tag{47}$$

can be obtained starting from the expansion of $S(\gamma)$ in powers of $\gamma - \bar{\gamma}$ and solving eq. (45) order by order, given that $n = O(\gamma - \bar{\gamma})$. The knowledge of the first k integer moments L_k is equivalent to the knowledge of

[13] In general, the Furstenberg theorem [31] guarantees that $\bar{\gamma}$ exists with probability 1 and is a non-random quantity, *i.e.* $\bar{\gamma} = \lim_{N\to\infty} \frac{1}{N} \langle \ln |P_N| \rangle$. This means that γ is a *self-averaging* quantity, and that $S(\gamma)$ must be a function peaked around $\bar{\gamma}$. Note that instead $|P_N| = e^{N\gamma}$, or an integer power of $|P_N|$ (including $|P_N|^{-1}$), is not in general a self-averaging quantity: it will be shown later in this section that $\langle |P_N| \rangle = e^{NL_1}$ and $\langle |P_N|^2 \rangle = e^{NL_2}$ where the L_n are $O(1)$, so that, as long as $L_2 > 2L_1$, $\langle (|P_N| - \langle |P_N| \rangle)^2 \rangle / \langle |P_N| \rangle^2 \sim e^{N(L_2 - 2L_1)} \gg 1$.

[14] We are assuming that $S(\gamma)$ is analytic and convex, so that the solution to the saddle point equation exists and is unique. Even if we cannot prove this assumption, it is strongly supported by numerical simulations, see Fig. 8. The same assumption guarantees that L_n is an analytic function of n and is at the basis of the replica method used in the next subsection.

[15] A zeroth-order approximation, corresponding to $\sigma = 0$, is $\pi_N(\gamma) = \delta(\gamma - \bar{\gamma})$, which gives the trivial result $L_n = n\bar{\gamma}$.

the first k derivatives of $S(\gamma)$ in $\gamma = \bar{\gamma}$ and allows us to reconstruct L_n up to a given order of approximation. Therefore, one possible way of investigation is to measure $S(\gamma)$ numerically, use a Gaussian fit to estimate $\bar{\gamma}$ and σ^2, and eventually compute the corrections coming from the cubic, quartic, ... terms of $S(\gamma)$. An illustrative numerical result for the function $S(\gamma)$ is plotted in Fig. 8 for $u = v = 0.24$, $w = 0.1$, where the deviation from Gaussianity is maximal. The Gaussian approximation becomes better as the critical point is approached. The insights gleaned from this numerical analysis become most powerful when combined with a different tool for computing the moments L_n, based on the so-called replica trick, to which we will turn in the next subsection.

6.2 Replica trick

A more efficient strategy is to compute the integer moments L_n directly with the help of the replica trick. For n a positive integer and for any sequence of matrices M_j, $j = 1, \cdots, N$, it is easy to show that

$$\left(\mathrm{Tr} \prod_j M_{q_j} \right)^n = \mathrm{Tr} \prod_j M_{q_j}^{\otimes n}, \tag{48}$$

where $\otimes$ is the tensor product. Then, if the M_j are independently and identically distributed,

$$\langle |P_N|^n \rangle = \left\langle \left(\mathrm{Tr} \prod_j M_{q_j} \right)^n \right\rangle = \mathrm{Tr} \left\langle \prod_j M_{q_j}^{\otimes n} \right\rangle = \mathrm{Tr} \prod_j \langle M_{q_j}^{\otimes n} \rangle = \mathrm{Tr} \, \langle M^{\otimes n} \rangle^N \sim \nu_n^N. \tag{49}$$

where ν_n is the largest eigenvalue of the matrix $\langle M^{\otimes n} \rangle$, which can be easily evaluated for n small. Thus one has, for positive integer n,

$$L_n = \ln \nu_n. \tag{50}$$

Knowing the function L_n for integers $0 < n \leq k$ allows one to compute the first k coefficients $l_1, \cdots, l_k$ of the n-expansion (47) simply by solving a linear system. This yields an approximate expression for $\bar{\gamma} = \lim_{n \to 0} \frac{dL_n}{dn} = l_1$ and for L_{-1}, which is the quantity we want to compute. Obviously the method assumes that L_n is an analytic function of n and would break down if there were a singularity at some value of n.

6.2.1 First moment

The simplest approximation is $L_n = l_1 n$. The coefficient l_1 is then equal to L_1 and is simply the logarithm of the largest eigenvalue of the matrix $\langle M \rangle = (A + B)/2$, that is,

$$\begin{aligned} \nu_1(u, v, w) &= \frac{1}{4} \left(2 + w + \sqrt{(2 - w)^2 - 4(u + v)} \right), \\ L_1(u, v, w) &= \ln \nu_1(u, v, w). \end{aligned} \tag{51}$$

This approximation is equivalent to neglecting the fluctuations of γ since

$$e^{NL_n} = \langle |P_N|^n \rangle = e^{nNL_1} = \langle |P_N| \rangle^n. \tag{52}$$

The function $\nu_1(u, v, w)$ has a singularity at

$$u + v = \left(\frac{2 - w}{2} \right)^2, \tag{53}$$

which intersects the critical surface only at the *critical point* $(u_c, v_c, w_c) \equiv (2/9, 2/9, 2/3)$. This point is therefore a good candidate for a singularity of L_{-1}, if it does not cancel at the next order.

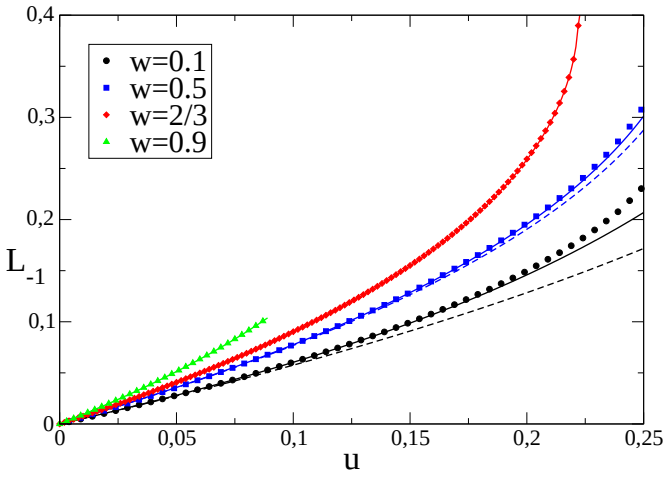

Figure 9: The numerical result for L_{-1} as a function of $u(=v)$ for $w = 0.1, 0.5, w_c, 0.9$. For $w \geq w_c = 2/3$, the simplest approximation $L_{-1} = -L_1$ (dashed line) works well. For $w = 0.1$ and 0.5, the Gaussian approximation, $L_{-1} = L_2 - 3L_1$ (continuous line), is needed to approximate the data better. For small w and $u \to 1/4$, it is clear that additional higher-order corrections are necessary, see also Fig. 8. However, the numerical data do not indicate a divergence of the derivative of L_{-1} with respect to u for $w \neq w_c$.

6.2.2 Second moment: Gaussian approximation

Including the first correction is equivalent to the Gaussian approximation and is obtained by considering $L_n = l_1 n + \frac{1}{2} l_2 n^2$ as in (46) above. One has

$$l_1 = \bar{\gamma} = 2L_1 - \frac{1}{2}L_2, \qquad l_2 = \sigma^2 = L_2 - 2L_1, \tag{54}$$

with $L_1 = \ln \nu_1$ as before and $L_2 = \ln \nu_2$, the logarithm of the largest eigenvalue of the 9×9 matrix $\langle M^{\otimes 2} \rangle = (A^{\otimes 2} + B^{\otimes 2})/2$. For our searched-for expression this implies $L_{-1} = L_2 - 3L_1$. We have calculated the eigenvalue ν_2 with the help of MATHEMATICA for $u = v$, but refrain from reporting it here, because it is long and not particularly illuminating. However, the expressions simplify considerably on the critical line $u = v = w - w^2$, where one has

$$\nu_2(w - w^2, w) = \begin{cases} w^2 & w > \frac{2}{3}, \\ \frac{1}{4}\left[2 - 2w + w^2 + \sqrt{4(1-w)^2 + w^2(2-3w)^2}\right] & w < \frac{2}{3}. \end{cases} \tag{55}$$

What is rather remarkable about this result is that for $w > 2/3$ we have $\nu_2 = \nu_1^2$, i.e. $L_2 = 2L_1$. It means that the approximation $L_n = nL_1$ is *exact*[16] on the critical line for $w > 2/3$. On this line we then obtain $L_{-1} = -\ln \nu_1 = -\ln w$.

More generally, we can write $L_{-1} = -L_1 + (L_2 - 2L_1) = -L_1 + \Delta L_2$ and study the behaviour of ΔL_2 close to the critical line. For later use in our scaling analysis, we consider two linearly independent types of perturbation away from a given point on the critical line, labelled by its w-coordinate w_0. The first one is

[16] To prove this statement one should prove that $\nu_n = \nu_1^n$ for all n. Although this ought to be possible, we have limited ourselves here to checking, by sampling random values on the critical line above $w > 2/3$, that it is true for n large but finite.

for $w = w_0 - \delta$ and $u = v = w - w^2$, thus describing motion along the critical line, for which we find

$$\Delta L_2 = \begin{cases} 0 & \text{for } w_0 > 2/3, \\ \kappa_1 \delta^2 + O(\delta^3) & \text{for } w_0 = 2/3, \\ \kappa_2 + \kappa_3 \delta + O(\delta^2) & \text{for } w_0 < 2/3. \end{cases} \tag{56}$$

The second one moves away from the critical line inside the diagonal plane $u = v$, and toward the interior of the singularity-free region according to $u = w_0 - w_0^2 - \epsilon$, yielding

$$\Delta L_2 = \begin{cases} \kappa_4 \epsilon^4 + O(\epsilon^5) & \text{for } w_0 > 2/3, \\ \kappa_5 \epsilon + \kappa_6 \epsilon^{3/2} + O(\epsilon^2) & \text{for } w_0 = 2/3, \\ \kappa_7 + \kappa_8 \epsilon + O(\epsilon^2) & \text{for } w_0 < 2/3 \end{cases} \tag{57}$$

where the κ_i in (56) and (57) are numerical constants. Interestingly, these corrections do not change the divergent term in the first derivatives of L_{-1} with respect to u and v at the critical point, which govern the presence or otherwise of an infinite-volume limit. Neither, since ν_2 according to (55) has no further singularities, can singularities appear at second order at points with $w_0 \neq 2/3$. In summary, since all correction terms give only finite contributions to the derivatives, it is clear that our first-order analysis already correctly identified $(u_c, v_c, w_c) = (2/9, 2/9, 2/3)$ as the only point at which an infinite-volume limit exists. This is confirmed by the numerical results for $L_{-1}(u, v = u, w)$ reported in Fig. 9.

Since ΔL_2 is proportional to ϵ at the critical point, we expect it to contribute to the calculation of the Hamiltonian. This would at first seem to necessitate an analytic determination for the eigenvalues of $(A^{\otimes 2} + B^{\otimes 2})/2$ for $u \neq v$, which is currently out of reach. Fortunately, all that is needed is a perturbative evaluation after inserting an ansatz for the scaling of u, v and w near the critical point, which is a perfectly feasible task we will perform in Sec. 9 below.

6.2.3 Higher moments: beyond the Gaussian approximation

The precision in determining L_{-1} can be improved further by computing L_3, L_4, etc. In Fig. 9 we report our numerical findings for L_{-1} (see appendix A-III), together with the first- and second-moment approximation just described. For $w > 2/3$ the first-order approximation is excellent, and the numerical deviations from $\Delta L_2 \sim 0$ for $w > 2/3$ and any value of u are very small. Around $w = 1/2$, the Gaussian correction starts to be observable. For $w < 1/2$ and $u \sim 1/4$, the correction is large, c.f. Fig. 8, and higher-order corrections have to be taken into account to correctly reproduce the numerical result.

For approaches to the critical point, we have found that ΔL_r, the incremental correction for the calculation of L_{-1} which results from adding the r'th one to that of the first $r-1$ moments, scales like $\epsilon^{r/2}$ and thus is not expected to contribute to the calculation of the Hamiltonian. We have confirmed this by perturbative calculations for L_3.

7 Continuum limit, canonical scaling and properties of the slices

As usual in dynamically triangulated models of quantum gravity, our next step will be to search for a continuum limit in which the details of the discretization procedure will be "washed out", and only universal, physical properties will remain. A necessary part of this limit is to take our short-distance cutoff, the edge length a, to zero, while keeping the *physical* spacetime volume $\mathcal{V}$ finite. This is only possible if the number of building blocks in the simplicial manifold (the *discrete* spacetime volume V) simultaneously goes to infinity. More precisely, we have to take the continuum limit following a trajectory (parameterized by a) in the coupling-constant space which ends up (for $a = 0$) in a point where the expectation value of the number of building blocks diverges, and which approaches this point in such a way that the physical volume stays finite. In other words, we have to renormalize the bare cosmological (and possibly other coupling) constants so that relevant physical quantities remain finite.

Our first step, the identification of a critical point with suitable properties, follows from the discussion of the previous section: the only point where the derivatives of the partition function[17] diverge is $(u_c, v_c, w_c) = (2/9, 2/9, 2/3)$. As a second step we will assume a canonical scaling, where the critical point is approached according to the canonical dimensions of the corresponding continuum coupling constants. To lowest non-trivial order in a, these are by definition

$$k \simeq k_c + \frac{a}{G}, \quad \ln x \simeq -\lambda_{b,c} - a^2 X, \quad \ln y \simeq -\lambda_{b,c} - a^2 Y, \quad \lambda \simeq \lambda_c + a^3 \Lambda, \tag{58}$$

for the inverse Newton, the two boundary cosmological and the bulk cosmological constants. In addition, a canonical scaling would require $T = at$ and $\mathcal{N} = aN$ for the time and spatial extensions.

Translated into the variables u, v and w (which were defined in (7)), the canonical scaling becomes

$$u = \frac{2}{9}\, e^{2ac_1/G - 2a^2 X - 2a^3 b_1 \Lambda}, \quad v = \frac{2}{9}\, e^{2ac_1/G - 2a^2 Y - 2a^3 b_1 \Lambda}, \quad w = \frac{2}{3}\, e^{-ac_2/G - a^3 b_2 \Lambda}. \tag{59}$$

Already without detailed inspection we can anticipate difficulties with the standard interpretation of the bulk and boundary cosmological constants as the couplings conjugate to the bulk volume and boundary areas. Since k scales with the lowest power of a when approaching the critical point, terms proportional to $1/G$ will be the ones which survive in the lowest-order expressions of the continuum limit, unless unexpected cancellations occur.

We can check this immediately by looking at what this particular choice of scaling implies for geometrical quantitites like the volume of sandwich geometries. As argued in the previous section, the second moment in the replica method only contributes to the next-to-leading order, which therefore we will need for the Hamiltonian, but not to recover the continuum expression for the volume. This means that as a starting point for our computation we can take the simple expression

$$Z_N \sim e^{-N \ln \nu_1(u,v,w)} \tag{60}$$

as the partition function of a sandwich geometry. Assuming canonical scaling for the three-volume and using previous definitions, we have

$$\begin{aligned} \langle \mathcal{V} \rangle &= \lim_{a \to 0} a^3 \langle V \rangle, \\ \langle V \rangle &= \left(-\frac{\partial}{\partial \lambda} \ln Z_N \right) = \left(2b_1 u \frac{\partial}{\partial u} + 2b_1 v \frac{\partial}{\partial v} + b_2 w \frac{\partial}{\partial w} \right) \ln Z_N, \end{aligned} \tag{61}$$

which after inserting the scalings (59) and taking the limit $a \to 0$ yields

$$\langle \mathcal{V} \rangle = a^{5/2} N \frac{2b_1 + b_2}{4\sqrt{(c_2 - 2c_1)/G}} \tag{62}$$

to lowest order in a. As expected, only the renormalized Newton constant G appears in the continuum expression for the volume. In addition, this expression indicates an anomalous scaling of either the time variable t or the variable N measuring the linear spatial extension. For example, if we insist on the canonical scaling $\mathcal{N} = aN$ for the finite continuum counterpart of N, we find that the volume goes to zero like $a^{3/2}$ instead of a as would be required for a canonical scaling $T = at$ of the time variable.

If instead we set $k = 0$ identically, corresponding to working with a bare action which only contains a cosmological term the sandwich volume scales canonically according to

$$\langle \mathcal{V} \rangle = a^2 N \frac{2b_1 + b_2}{4\sqrt{X + Y}} = a\mathcal{N} \frac{2b_1 + b_2}{4\sqrt{X + Y}}. \tag{63}$$

[17] Remember that the average volume is given by the derivative of the logarithm of the partition function with respect to the bare cosmological constant, which translates into a linear combination of $u\frac{\partial}{\partial u}$, $v\frac{\partial}{\partial v}$ and $w\frac{\partial}{\partial w}$, see (61).

Since we do not want to touch the canonical scaling of the three-volume, which would affect the interpretation of the model in a fundamental way, one possible solution is to choose the constants c_i such that $c_2 = 2c_1$ and the order-a terms cancel each other. In this case we would obtain

$$\langle \mathcal{V} \rangle = a^2 N \frac{2b_1 + b_2}{4\sqrt{X + Y - \frac{3}{4}c_2^2/G^2}}. \tag{64}$$

The scaling now *is* canonical, and the sandwich volume is governed by both the boundary cosmological constants and the Newton constant. We will see below that related issues appear when we try to derive the continuum Hamiltonian.

Another quantity one can consider is the total, integrated scalar curvature $\mathcal{R}_{tot} \equiv \int d^3x\sqrt{g}\ \mathcal{R}$. Its counterpart at the discrete level is exactly the term R_{tot} multiplying k in the gravitational action, for which we have used the standard Regge prescription. We can express the average total curvature as a derivative with respect to k of the partition function, and then take the continuum limit. The analogues of relations (61) are given by

$$\begin{aligned} \langle \mathcal{R}_{tot} \rangle &= \lim_{a\to 0} a\langle R_{tot} \rangle, \\ \langle R_{tot} \rangle &= \frac{\partial \ln Z_N}{\partial k} = -c_3 N + \left(c_1 \left(2u\frac{\partial}{\partial u} + 2v\frac{\partial}{\partial v} \right) - c_2 w \frac{\partial}{\partial w} \right) \ln Z_N. \end{aligned} \tag{65}$$

Since our spacetime sandwiches in the continuum limit have only infinitesimal thickness and thus infinitesimal volume, it is more appropriate to work with the average curvature per volume,

$$\bar{\mathcal{R}} \equiv \frac{\langle \mathcal{R}_{tot} \rangle}{\langle \mathcal{V} \rangle}. \tag{66}$$

It is a well-known feature of dynamically triangulated models of gravity that this quantity generically diverges like a^{-2}, unless specific cancellations occur. We find here not only the same behaviour, but even the same algebraic expression to leading order, namely,

$$\bar{\mathcal{R}} = \frac{1}{a^2}\left(\frac{2c_1 - c_2}{2b_1 + b_2} \right), \tag{67}$$

regardless of whether we assume the scaling $k = 0$, or the canonical $k \simeq k_c + a/G$. However, in line with our earlier remarks, *if* one makes the choice[18] $2c_1 = c_2$, a different, less divergent, behaviour is found. Combining this condition and canonical scaling, we obtain

$$\bar{\mathcal{R}} = \frac{1}{a}\left(\frac{3c_2^2/G}{4b_1 + 2b_2} + \left(\frac{c_2 - 4c_3}{2b_1 + b_2} \right) \sqrt{X + Y - \frac{3}{4}c_2^2/G^2} \right). \tag{68}$$

For $k = 0$ we find instead

$$\bar{\mathcal{R}} = \frac{1}{a}(c_2 - 4c_3)\frac{\sqrt{X+Y}}{2b_1 + b_2} - \frac{3}{2}\left(\frac{c_2}{2b_1 + b_2} \right)(X + Y). \tag{69}$$

We will encounter somewhat similar scaling relations in the discussion of the quantum Hamiltonian in Sec. 9 below.

[18] This can be achieved by fixing the finite relative factor r between the time- and space-like (squared) edge lengths of the triangulations (c.f. appendix A-I). Using eq. (A-7), it corresponds to taking $r \simeq 0.724$.

8 Transfer matrix for areas

One way to construct the propagator for finite times t of a statistical model is by iteration of the transfer matrix $\hat{T}$, which in our case would take the form $\langle g_2|\hat{T}^t|g_1\rangle$. Although the determination of the complete transfer matrix for our three-dimensional model is out of reach, we have already argued in Sec. 2.2 that most of the detailed dependence of the propagator on the boundary geometries g_i will be dynamically irrelevant, because of the absence of local degrees of freedom in the three-dimensional gravity theory. Following [18], keeping track only of the boundary areas A_i in the one-step propagator as we have been doing throughout this work, should be enough[19] to determine the finite-time behaviour of the propagator in the continuum limit. Introducing the "area states"

$$|A\rangle = \frac{1}{\sqrt{\mathcal{N}(A)}} \sum_{g_{|A}} |g_{|A}\rangle, \tag{70}$$

where $\mathcal{N}(A)$ is the number of triangulations of a given area A and $g_{|A}$ any triangulation with a given total number of triangles A, we obtain that

$$\begin{aligned} Z(x, y, \Delta t = 1) &= \sum_{A_1, A_2} x^{A_1} y^{A_2} \sum_{g_{|A_1}, g_{|A_2}} \langle g_{|A_2}|\hat{T}|g_{|A_1}\rangle = \\ &= \sum_{A_1, A_2} x^{A_1} y^{A_2} \langle A_2|\hat{T}|A_1\rangle \sqrt{\mathcal{N}(A_1)\mathcal{N}(A_2)}. \end{aligned} \tag{71}$$

Assuming now in line with our earlier reasoning (see also [18]) that

$$\langle A_2|\hat{T}|g_{|A_1}\rangle - \langle A_2|\hat{T}|g'_{|A_1}\rangle \to 0 \qquad \text{for} \qquad A_2, A_1 \to \infty, \tag{72}$$

for all pairs g, g' of boundary geometries of the same area, the completeness relation

$$\int dA |A\rangle\langle A| = \mathbb{I} \tag{73}$$

holds in the large-area limit and we can use $\langle A_2|\hat{T}|A_1\rangle$ as our transfer matrix. One remaining problem is the appearance of the square-root term $\sqrt{\mathcal{N}(A_t)\mathcal{N}(A_{t+1})}$ in (71), which we will have to deal with either before or after performing the inverse Laplace transform of $Z(x, y, \Delta t = 1)$. Given that the number of triangulations of a given area A scales like

$$\mathcal{N}(A) \sim A^{-\alpha} e^{\lambda_0 A}, \tag{74}$$

with $\alpha = 1/2$ as we will show at the end of this section, one possibility is to apply to $Z(x, y, \Delta t = 1)$ a fractional derivative operator

$$\sum_{A_1, A_2} x^{A_1} y^{A_2} \langle A_2|\hat{T}|A_1\rangle = \left(\frac{\partial}{\partial \ln x}\right)^{\alpha/2} \left(\frac{\partial}{\partial \ln y}\right)^{\alpha/2} Z(x, y, \Delta t = 1) \ . \tag{75}$$

There are several definitions of fractional derivatives in the literature; what we need here is an operator D_x^α such that $D_x^\alpha e^{Ax} = A^\alpha e^{Ax}$, so that applying $D_{\ln x}^{\alpha/2} D_{\ln y}^{\alpha/2}$ term by term to (71) we get rid of the entropy factors (the remaining exponential term $e^{\lambda_0 A}$ is unproblematic since it only shifts the location of the critical point). We need yet another property for our fractional derivative, namely, a "chain rule", since the final expression for $Z(x, y, \Delta t = 1)$ will involve some function of x and y. In particular, since the final expression is expanded in powers of $\ln x$, it would be nice if the derivative would act on powers with the simple rule $D_x^\alpha x^n \propto x^{n-\alpha}$. An explicit representation of a fractional derivative operator with the desired properties exists and is reviewed in appendix A-IV.

[19] Possibly up to an additional dependence on global Teichmüller parameters.

Unfortunately, at the relevant value $\alpha = 1/2$, for some terms in the final expression for $Z(x, y, \Delta t = 1)$ the fractional derivatives suffer from convergence problems. These can be circumvented in a somewhat *ad-hoc* fashion by integrating by parts or by introducing a regularization in the fractional integrals, which should be removed only after the ordinary derivative has been applied. (As explained in appendix A-IV, the fractional derivative is actually defined as an ordinary derivative acting on a fractional integral.)

A cleaner alternative to get the correct Hamiltonian is to first work out the inverse Laplace transform and then identify the contribution coming from the entropy factor and remove it. This method on the other hand requires some special care for the following reason. Starting from (71), keeping only the two lowest orders in a (see (3)), and doing an inverse Laplace transform will produce $\mathcal{N}(A_1)\delta(A_1 - A_2)$ at the lowest order and some differential operator acting on $\delta(A_1 - A_2)$ at the next order. If we divided this operator by $\mathcal{N}(A_t)$ to obtain the Hamiltonian, we would make a mistake since at next-to-leading order $A_2 \simeq A_1 + a\delta A$, which needs to be taken into account. To do so let us rewrite the coefficients of the power series (71) as follows:

$$\begin{aligned}\langle A_2|\hat{T}|A_1\rangle\sqrt{\mathcal{N}(A_1)\mathcal{N}(A_2)} &= \langle A_2|\sqrt{\mathcal{N}(\hat{A})}\;\hat{T}\;\sqrt{\mathcal{N}(\hat{A})}\;|A_1\rangle = \\ &= \langle A_2|\mathcal{N}(\hat{A})\hat{T}|A_1\rangle + \langle A_2|\sqrt{\mathcal{N}(\hat{A})}\left[\hat{T},\sqrt{\mathcal{N}(\hat{A})}\right]|A_1\rangle = \\ &= \mathcal{N}(A_2)\langle A_2|(1-a\hat{H})|A_1\rangle - a\sqrt{\mathcal{N}(A_2)}\langle A_2|\left[\hat{H},\sqrt{\mathcal{N}(\hat{A})}\right]|A_1\rangle + O(a^2),\end{aligned} \tag{76}$$

where we have introduced the area operator $\hat{A}|A_1\rangle = A_1|A_1\rangle$. If we define the auxiliary Hamiltonian $\hat{H}'$ by

$$\langle A_2|\hat{T}|A_1\rangle\sqrt{\mathcal{N}(A_1)\mathcal{N}(A_2)} := \mathcal{N}(A_2)\langle A_2|(1-a\hat{H}')|A_1\rangle + O(a^2), \tag{77}$$

we can invert (77) by using (76) to find the real Hamiltonian

$$\hat{H} = \hat{H}' + \sqrt{\mathcal{N}(\hat{A})}\left[\hat{H}', \frac{1}{\sqrt{\mathcal{N}(\hat{A})}}\right]. \tag{78}$$

It turns out that also with this method convergence problems appear in some of the inverse Laplace transforms to be performed. Fortunately, since the divergences in the fractional derivative method and in the auxiliary Hamiltonian method appear in different terms, they can be regularized consistently by requiring the end result in both methods to agree (see appendix A-IV).

We conclude this section by showing that $\alpha = 1/2$ in the scaling relation (74) for the number of boundary geometries. The entropy of this class of triangulations can be deduced from its leading critical behaviour. Summing over all the triangulations with a cosmological weight – as is appropriate for evaluating the gravitational partition function in two dimensions – one has

$$\sum_{\mathcal{T}} e^{-\lambda A} \sim \sum_{A} A^{-\alpha} e^{-(\lambda-\lambda_0)A} \sim (\lambda - \lambda_0)^{\alpha-1}. \tag{79}$$

Of course, the boundaries of our model are nothing but standard (1+1)-dimensional causal dynamical triangulations with periodically identified time. For precisely this ensemble we have already established earlier the relation (14), with whose help we will now be able to find α analytically. Summing over t to include all triangulations (and including a factor of $1/2^t$, which is necessary for convergence[20]), we simply get

$$\sum_t \frac{1}{2^t} Z_t^{2d} = \frac{1}{\ln 2 + \ln \lambda_+(u)} \sim \frac{1}{\sqrt{1-4u}}, \tag{80}$$

[20]The normalization is needed in order to take the continuum limit of the partition function at fixed continuum time T. This can be understood in the following way. If we start with the generating function (18) for the transfer matrix, we find to leading order *twice* the identity operator in the continuum limit. Consequently, if we iterate (18) t times, we will get a multiplicative factor 2^t, which has to be removed if we want to obtain the continuum T-propagator.

since there is no power-like subleading behaviour in t. Comparing with (79), we deduce that for the (1+1)-dimensional boundaries we have $\alpha = 1/2$.

9 The Hamiltonian

The continuum dynamics of the model is encoded in the Hamiltonian operator, which can be derived by taking the continuum limit of the transfer matrix, as we explained before. Starting from Eq. (28), we obtain

$$Z(x, y, \Delta t = 1) = \sum_N (2e^{-\gamma'})^N e^{N L_{(-1)}(u,v,w)}, \tag{81}$$

where we have defined $e^{-\gamma'} = be^{-\gamma}$ to allow for a multiplicative renormalization of the partition function at fixed N, in analogy with the two-dimensional case (80). The continuum limit is obtained for $u \to u_c$, $v \to v_c$, $w \to w_c$, if we tune $\gamma' = \log 2 + L_{(-1)}(u_c, v_c, w_c)$, yielding

$$Z(x, y, \Delta t = 1) = \sum_N e^{N[L_{(-1)}(u,v,w) - L_{(-1)}(u_c,v_c,w_c)]} \sim \frac{1}{L_{-1}(u_c, v_c, w_c) - L_{-1}(u, v, w)}, \tag{82}$$

for the leading term. To derive the quantum Hamiltonian in the "X-representation", we substitute the known function $L_{-1}(u, v, w)$ as well as an ansatz for the scaling relations into the evolution equation

$$\psi(x, t + 1) = \oint \frac{dy}{2\pi i y} Z(x, y^{-1}, \Delta t = 1)\psi(y, t) \tag{83}$$

for the wave function (remember that x and y were absorbed in u and v), and evaluate its continuum limit to order a, namely,

$$\left(1 - a\hat{H}_X + \mathcal{O}(a^2)\right)\psi(X, T) = -a^2 \int_{-i\infty+\mu}^{+i\infty+\mu} \frac{dY}{2\pi i} Z(X, -Y; a)\psi(Y, T). \tag{84}$$

In (84), μ is chosen such that the integration contour lies to the right of the singularities of $\psi(Y, T)$ and to the left of those of $Z(X, -Y; a)$, around which we have to close it.

To show that to lowest order the identity operator is reproduced and to extract the Hamiltonian at the next order, we clearly need the first two orders in a of $L_{-1}(u, v, w) - L_{-1}(u_c, v_c, w_c)$. As discussed in Sec. 6.2 above, to get the order-a^2 terms right we need to use the replica trick up to the second moment approximation, *i.e.* $L_{-1} = L_2 - 3L_1$. It does not matter that we do not have a closed analytic expression available, since we will only need the expansion up to order a^2. This can be found perturbatively around the solution at the critical point (where we *can* solve for the eigenvalues of $(A^{\otimes 2} + B^{\otimes 2})/2$), with the eigenvalue problem perturbed in accordance with the chosen scaling of coupling constants.

In anticipation of difficulties with the scaling of k we first discuss the results for $k = 0$. Given the analytic expression of L_1 and after computing

$$L_2(X, Y, G, \Lambda) = \ln\left(\frac{4}{9} + a\frac{4}{9}\sqrt{X + Y} + \frac{a^2}{27}\left(\frac{4X^2 + 5XY + 4Y^2}{X + Y} + \frac{(4b_1 + 2b_2)\Lambda}{\sqrt{X + Y}}\right)\right) + O(a^3), \tag{85}$$

we have all we need to calculate the partition function, resulting in

$$a^2 Z(X, -Y; \Lambda) = \frac{2a}{\sqrt{X - Y}} + a^2\left(\frac{5}{6} + \frac{XY}{(X - Y)^2} - \frac{\Lambda}{(X - Y)^{3/2}}\right) + O(a^3), \tag{86}$$

where we have absorbed a finite numerical factor in Λ. This expression is in perfect agreement with our previous discussion, since due to the entropy factor $\mathcal{N}(A) \sim A^{-1/2}e^{\lambda_0 A}$ from the boundaries we expect the leading term to have an inverse square-root singularity if the transfer matrix is to reduce to the identity

at lowest order. Using the fractional derivative method before the integration in (84) or, alternatively, the method of the auxiliary Hamiltonian one finds

$$\hat{H}_{\mathcal{A}} = -\mathcal{A}^{\frac{3}{2}}\frac{\partial^2}{\partial\mathcal{A}^2} - \frac{3}{2}\mathcal{A}^{\frac{1}{2}}\frac{\partial}{\partial\mathcal{A}} - \frac{1}{16}\frac{1}{\mathcal{A}^{\frac{1}{2}}} + \Lambda\ \mathcal{A} \tag{87}$$

for the quantum Hamiltonian in the "$\mathcal{A}$-representation" (with $\mathcal{A}$ denoting the (finite) continuum area). This looks like a bona-fide Hamiltonian, with a second-order kinetic term and a potential term depending on the cosmological constant. In the absence of a dimensionful Newton coupling G, the factor $\mathcal{A}^{\frac{1}{2}}$ multiplying the kinetic term must be present for dimensional reasons. Note also the appearance of the factor $3/2$ in front of the first-order derivative, ensuring the self-adjointness of the Hamiltonian with respect to the trivial $d\mathcal{A}$-measure. By introducing a new variable

$$L = 4\sqrt{\mathcal{A}} \tag{88}$$

and simultaneously defining new wave functions[21]

$$\phi(L) = \frac{\sqrt{2L}}{4}\psi(\frac{L^2}{16}), \tag{89}$$

the Hamiltonian becomes

$$\hat{H}_L = -L\frac{\partial^2}{\partial L^2} - \frac{\partial}{\partial L} + \frac{\Lambda}{16}L^2, \tag{90}$$

with the $1/L$-term having disappeared from the potential. Apart from the cosmological term, which has the appropriate dimension for a (2+1)-dimensional Hamiltonian, this is exactly the quantum Hamiltonian of the (1+1)-dimensional CDT model [1] (see also [9] for a similar transformation of variables).

Since by setting $k = 0$ we have not included any spacetime-curvature term in the discrete action, it is clear that the kinetic terms in (87) and (90) have their origin in the "entropy" of configurations, or, using a continuum language, in the non-trivial path integral measure underlying the dynamically triangulated model. This is also underlined by the absence of such a kinetic term from a related (1+2)-dimensional model considered and solved in [28], which uses the same product structure as our model, but works instead with a *fixed*, flat base manifold. Rather intriguingly, this gravity-inspired model (for finite t) can be related through an inversion formula to a problem of hard hexagons on a regular triangulation. Its one-step propagator can be seen to resurface in our model as contributing just one of the terms in the partition function, namely, $\tilde{Z}_N = 1/Tr(AB)^{N/2}$. Solving the model in the large-N limit does not require the replica trick, and simply leads to $\tilde{Z}_N \sim 1/\lambda_{max}^{N/2}$, where λ_{max} is the largest eigenvalue of the matrix AB. It is straightforward to extract the Hamiltonian, which only contains a term proportional to the area, and no derivatives, which implies that the area is not a dynamical quantity in the continuum limit[22].

Returning to the analysis of our model, the case with $k \neq 0$ raises issues similar to those already encountered when computing the spacetime volume and curvature. The a/G-term dominates the continuum

[21] With such a change of wave functions we make sure that the measure is preserved, in the sense that

$$\int d\mathcal{A}\ \psi_1(\mathcal{A})\psi_2(\mathcal{A}) = \int dL\ \phi_1(L)\phi_2(L).$$

Note that we also require

$$\int d\mathcal{A}\ \psi_1(\mathcal{A})\hat{H}_{\mathcal{A}}\psi_2(\mathcal{A}) = \int dL\ \phi_1(L)\hat{H}_L\phi_2(L),$$

which implies

$$\hat{H}_L = \hat{H}_{\mathcal{A}\to L} + \sqrt{L}\left[\hat{H}_{\mathcal{A}\to L}, \frac{1}{\sqrt{L}}\right],$$

with the $\mathcal{A}$ in the Hamiltonian substituted according to (88).

[22] The mapping to the hard hexagon model of [28] suggested a fractal dimension $d_f = 12/5$ for the (1+2)-dimensional simplicial complexes. The relation with our results for the associated one-step propagator is currently unclear. We conjecture that in our model, where we sum over all base triangulations, the fluctuations of the base serve as a stabilizer for the geometry and lead to an effective, non-anomalous dimension $d_f = 3$ for finite times.

limit, giving rise to

$$a^2 Z(X,-Y;G,\Lambda) = \frac{2a^{3/2}}{3\sqrt{(c_2-2c_1)/G}} + a^2 \frac{(6c_1-5c_2+8c_3)/G - 4\sqrt{4X-4Y-3(c_2/G)^2}}{(36c_1-18c_2)/G} + O(a^{5/2}), \quad (91)$$

which is difficult to interpret within the scheme of the previous section (and to this order does not even contain any reference to the cosmological constant Λ!) Things simplify somewhat once we choose $c_2 = 2c_1$, in which case we obtain

$$a^2 Z(X,-Y;G,\Lambda) = \frac{2a}{4c_3 - c_2 + \sqrt{X - Y - \frac{3}{4}\left(\frac{c_2}{G}\right)^2}} + O(a^2). \quad (92)$$

We have not bothered to include the next term in the expansion, because already the lowest-order expression gives nothing like the desired form $\mathcal{N}(\mathcal{A})\delta(\mathcal{A}-\mathcal{A}')$ upon performing an inverse Laplace transform. It is not totally inconceivable that the offensive terms in (92) could still be "argued away". Note that we have encountered the numerical term $(4c_3 - c_2)$ previously in the expressions (68) and (69) for the average curvature. In particular, *if* we had a good reason for why $(4c_3 - c_2)$ could be set to zero (which we currently do not), it would imply that in the case $k = 0$ the average curvature was turned into a finite expression. However, even if $(4c_3 - c_2)$ could be made to vanish, it would still leave us with the problem of having to absorb the shift in the location of the singularity from $Y = X$ to $Y = X - \frac{3}{4}\left(\frac{c_2}{G}\right)^2$. In terms of the $\mathcal{A}$-representation, the shift can be related to an overall multiplicative operator, which replaces the simple transfer matrix $e^{-a\hat{H}_\mathcal{A}}$ by $e^{-a\hat{H}_\mathcal{A}} e^{\frac{3}{4}\left(\frac{c_2}{G}\right)^2 \hat{\mathcal{A}}}$. This might be related to a redundancy among the renormalized couplings of the model inherent in the ansatz (58), (59), but we have not yet been able to make the relation precise.

10 Conclusions

In this paper, we have for the first time derived a continuum Hamiltonian from a three-dimensional quantum gravity model in terms of Causal Dynamical Triangulations. This was made possible by restricting ourselves to a subclass of all triangulations, which possess a product structure in the spatial direction, in addition to the usual product structure in the time direction underlying the causal nature of the model. This restriction enabled us to apply a number of analytical methods, including the inversion formula, a random matrix formulation and the replica trick, to solve the one-step propagator with free boundary conditions and then perform its continuum limit. This led to an explicit expression for the quantum Hamiltonian (87) in $\mathcal{A}$-space, with wave functions depending on the area $\mathcal{A}$ of two-dimensional spatial slices.

Taking into account the special, topological character of three-dimensional pure gravity, we have argued that for obtaining the full dynamics of the theory, it is sufficient to keep track of only a finite number of boundary data when deriving the model's transfer matrix from the one-step propagator, and sum over everything else. This should not be confused with an approach where the remaining degrees of freedom (essentially the conformal mode of the metric) are fixed at the outset. In our model, all of these are still present, but are summed over in the discrete path integral. For simplicity, what we have done in the present piece of work is to keep track of only a single variable, the volume (area) of the two-dimensional universe. Because of the cylindrical topology of our spatial slices, we expect there to be one additional Teichmüller parameter, corresponding to the ratio between the area of the cylinder and the length of the cycle (the boundary of the cylinder). To include this parameter in our model will require to separately keep track of the number of matrices A and B (for the incoming and outgoing cylinder) in the traces, instead of only their sum N, as we have done here. This task is in principle solvable with the help of the so-called microcanonical method [32], based on an idea similar to that of the replica trick. This issue is currently under consideration, with some progress reported in [33].

The fact that we have derived a non-trivial three-dimensional dynamics does *a posteriori* justify our restriction to a subclass of all three-dimensional Lorentzian triangulations. Since the continuum limit we

have identified was obtained by setting the bare inverse Newton constant to zero, it is clear that the resulting continuum Hamiltonian describes the "collective" effect of the quantum fluctuations we have summed over in the path integral, and which elsewhere we have called the entropy of the model. In particular, the net effect of these fluctuations is to generate a kinetic term for the area which makes the Hamiltonian *bounded below*, and therefore has the opposite sign from the corresponding term for the "global conformal mode" in the gravitational action. This further supports a mechanism already observed elsewhere in CDT models in three and four dimensions, namely, the presence of contributions from the path integral measure compensating for the divergence due to the conformal mode of the Euclidean gravitational action.

There is a (small) price we are paying for using the additional constraint of a double product structure for the triangulations, which after all was not motivated by physics, but simply by the desire to be able to apply a number of special solution techniques. The application of the inversion formula implies that we are evaluating first the limit of infinitely many building blocks in *one* of the spatial directions (the "height" of the towers), and only then the corresponding limit in the complementary direction, corresponding to what we have called the large-N limit. The effect of taking these two limits in sequence, and not simultaneously, is that the u-w-diagram (Fig. 7), which describes the behaviour *after* taking the first of the infinite sums, has only a single point at which an infinite-volume limit can be defined. This is in contrast to the corresponding phase diagram for three-dimensional CDT, which has an entire critical line $\lambda_c(k)$ along which the infinite-volume limit can be taken.

The analytic solution found here has also highlighted a problem with the scaling of Newton's constant, which has already been encountered in previous analyses of the phase structure of three-dimensional CDT models [20]. The issue is that a standard canonical, additive renormalization of Newton's constant as in (58) does not seem to lead to a good continuum limit, simply because the term containing the renormalized Newton constant G has the lowest order in a, and dominates everything else. The only way so far in which we have managed to obtain a nontrivial continuum limit was by setting $k = 0$, which implies that the Newton constant does not play a dynamical role, which is of course compatible with the absence of local gravitational excitations in three dimensions. We believe a deeper understanding of the relation between certain scalings of the coupling constants and that of physically relevant quantities, like the curvature discussed in Sec. 7 above would be useful, and potentially relevant for a better understanding of the analogous issues in four dimensions. – Even if this and other issues still remain open, we think that the work presented here presents an important step in the analytical understanding of CDT models in $d > 2$ dimensions.

Acknowledgements. We thank R. Costa-Santos for discussions during the early stages of the project. D.B. and R.L. are partially supported through the European Network on Random Geometry ENRAGE, contract MRTN-CT-2004-005616. R.L. acknowledges support by the Netherlands Organisation for Scientific Research (NWO) under their VICI program. D.B. thanks the Laboratoire de Physique Théorique (LPT) of the ENS in Paris, and the Service de Physique Théorique (SPhT), CEA Saclay, and F.Z. thanks the Institute for Theoretical Physics of Utrecht University for hospitality during some stages of the preparation of this work.

A-I The discrete action

We derive in this appendix the exact expression for the action of our model. All the definitions and necessary ingredients were already introduced in [2], here we just recall and use them to derive the precise expression for our particular case. We start from the Einstein-Hilbert action plus a Gibbons-Hawking boundary, that is,

$$\mathcal{S} = \int_M d^3x\sqrt{g(x)}\left(\Lambda - \frac{R(x)}{2G}\right) + \frac{1}{G}\int_{\partial M} d^2x\sqrt{h(x)}K(x), \tag{A-1}$$

and then use Regge's prescription for the corresponding quantities on a simplicial manifold [34, 35] to obtain the discrete action

$$\mathcal{S} \to S = \Lambda_b \sum_{\sigma_3} V_{\sigma_3} - \frac{1}{G_b}\sum_{\sigma_1\in\dot{M}} V_{\sigma_1}(2\pi - \sum_{\sigma_3\supset\sigma_1}\theta_{\sigma_3\triangleright\sigma_1}) - \frac{1}{G_b}\sum_{\sigma_1\in\partial M} V_{\sigma_1}(\pi - \sum_{\sigma_3\supset\sigma_1}\theta_{\sigma_3\triangleright\sigma_1}), \tag{A-2}$$

where σ_n is an n-dimensional simplex, V_{σ_n} its volume, $\dot{M}$ is the interior of the simplicial manifold and ∂M its boundary, $\theta_{\sigma_3\triangleright\sigma_1}$ is the dihedral angle of σ_3 at σ_1, and the subscript b on the coupling constants stands for *bare*.

In Dynamical Triangulations things simplify considerably because the edge lengths are held fixed. In the old, Euclidean models one would have only a single type of building block in any dimension, since all the edge lengths were chosen equal. In CDT the Lorentzian nature of the model allows us to have two different types of edge lengths, corresponding to time- and space-like directions. Because of the way the causal gluing rules are implemented, what used to be a space-like and what used to be a time-like link can still be distinguished after having mapped a Lorentzian triangulation to its Euclidean counterpart. Let us define the ratio $r = l_t^2/l_s^2$, where l_t^2 denotes the squared edge length for all time-like links, and l_s^2 that for all space-like ones. Its allowed range in the Euclidean signature is $r > \epsilon > 0$, where ϵ is a positive constant, which is the lower bound of the triangular inequalities and depends on the number of dimensions d ($\epsilon = 1/4$ for $d = 2$, $\epsilon = 1/2$ for $d = 3$ and $\epsilon = 7/12$ for $d = 4$). An analytic continuation of r in the complex plane to negative values defines the (inverse) "Wick rotation" in CDT. Throughout this work, we will stick to positive values for ϵ, corresponding to a Euclideanized, real partition function.

In (2+1) dimensions we have precisely two different kinds of building blocks, tetrahedra with three space-like and three time-like edges, and tetrahedra with two space-like and four time-like edges. We will use the notation N_{ij} for the number of (i, j)-simplices of dimension $i + j - 1$ having i vertices in a constant-time slice t and j vertices in the subsequent one at time $t + 1$. The Regge action (A-2) in this case becomes

$$\begin{aligned} S =& \Lambda_b a^3\left(V_{2,2}N_{2,2} + V_{3,1}(N_{3,1} + N_{1,3})\right) - \frac{a}{G_b}\Big(2\pi\sqrt{r}N_{1,1}^{(\dot{M})} + \pi\sqrt{r}N_{1,1}^{(\partial M)} + \\ &- \sqrt{r}\left[4\theta_{2,2}^t N_{2,2} + 3\theta_{1,3}^t(N_{1,3} + N_{3,1})\right] + \pi(N_{2,0} + N_{0,2}) + \\ &- \left[2\theta_{2,2}^s N_{2,2} + 3\theta_{1,3}^s(N_{1,3} + N_{3,1})\right]\Big), \end{aligned} \tag{A-3}$$

where we have distinguished the dihedral angles at time-like and space-like links by the superscripts t and s. Relevant volumes and angles are easily found to be

$$V_{2,2} = \frac{\sqrt{2r-1}}{6\sqrt{2}}, \quad V_{3,1} = \frac{\sqrt{3r-1}}{12}, \tag{A-4}$$

$$\begin{aligned} \cos\theta_{1,3}^s &= \frac{1}{\sqrt{3}\sqrt{4r-1}}, \quad \cos\theta_{1,3}^t = \frac{2r-1}{4r-1}, \\ \cos\theta_{2,2}^s &= \frac{4r-3}{4r-1}, \quad \cos\theta_{2,2}^t = \frac{1}{4r-1}. \end{aligned} \tag{A-5}$$

Finally, using Euler's formula and the Dehn-Sommerville relations for triangulated manifolds with boundary[23], we arrive at the expression

$$S = \alpha(N_{13} + N_{31}) + \beta N_{22} + \gamma N \tag{A-6}$$

for the discrete action, where α, β and γ depend on the dimensionless bare coupling constants λ and k according to

$$\begin{aligned}
\alpha &= \left(-\pi\sqrt{r} + 3\sqrt{r}\arccos\frac{2r-1}{4r-1} - \frac{3}{2}\pi + 3\arccos\frac{1}{\sqrt{3}\sqrt{4r-1}}\right)k + \frac{\sqrt{3r-1}}{12}\lambda = -c_1 k + b_1\lambda, \\
\beta &= \left(-2\pi\sqrt{r} + 4\sqrt{r}\arccos\frac{1}{4r-1} + 2\arccos\frac{4r-3}{4r-1}\right)k + \frac{\sqrt{2r-1}}{6\sqrt{2}}\lambda = c_2 k + b_2\lambda, \\
\gamma &= \left(6\pi\sqrt{r} - \pi\right)k = c_3 k.
\end{aligned} \tag{A-7}$$

A-II The inversion formula

The proof of the inversion formula in (2+1) dimension (for a fixed sequence S_N of N blue and red towers) proceeds very similarly to that in (1+1) dimensions given in [28]. We first switch to the dual picture of a triangulation, and assign a weight u or v to each horizontal edge, depending on its colour, and a weight w to each red-blue intersection, as depicted in Fig. 6 above. Next, we decompose a given configuration into a

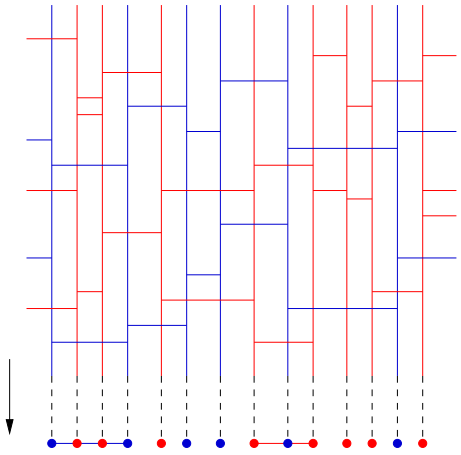

Figure 10: Decomposing the dual picture of a sandwich geometry into a sequence of projections onto its one-dimensional base line. The projection is obtained by letting the "bottom layer" of the heap of pieces, consisting of its lowest-lying edges, drop down to the horizontal line at the base. Each such projection defines a hard-dimer configuration on the horizontal line.

sequence of projections onto the base, as illustrated in Fig.10. Such a projection gives rise to a hard-dimer configuration, if by a dimer we simply mean an edge linking two nearest vertices of the same colour. The "hardness" refers to the fact that any vertex of the base can be occupied by at most one dimer, incorporating a mutual avoidance of dimers. Such a construction is possible because the dual graph is a heap of pieces. One may think of the vertical lines in Fig. 10 as tracks along which the horizontal edges can slide up and down, with the only restriction of not being allowed to touch or pass each other. Using this decomposition, we can write the partition function $Z_T(t)$ as

$$Z_{S_N}(u,v,w) = \sum_{\text{hard dimer config. } C} u^{|C|_b} v^{|C|_r} w^{|\cap C|} Z^{(C)}_{S_N}(u,v,w), \tag{A-8}$$

[23]Note that the boundary of our "sandwiches" of three-dimensional spacetime (the product of a finite cylinder with an interval), which has space-like as well as time-like components, is connected and has the topology of a torus.

where the sum extends over all hard-dimer configurations C on the one-dimensional lattice (including the empty configuration). The numbers $|C|_b$ and $|C|_r$ count the blue and red dimers in C, and $|\cap C|$ the crossings between dimers and sites of different colour in the configuration C. For fixed C, $Z^{(C)}(u,v,w)$ is the restricted partition function involving those configurations having projection C, and from which we have factored out the weight $u^{|C|_b}v^{|C|_r}w^{|\cap C|}$ of the projected part. More generally, we have the relations

$$u^{|D|_b}v^{|D|_r}w^{|\cap D|}Z_{S_N}(u,v,w) = \sum_{C\supset D} u^{|C|_b}v^{|C|_r}w^{|\cap C|}Z^{(C)}_{S_N}(u,v,w), \tag{A-9}$$

valid for any hard-dimer configuration D (eq. (A-8) corresponding to $D=\emptyset$). This expresses the fact that by completing any dual geometric configuration under consideration by a given row of horizontal edges (corresponding to a hard-dimer configuration D), one builds each configuration having a projection containing D, i.e. having D as a sub-configuration exactly once, see Fig.11. Let us now rewrite (A-9) as

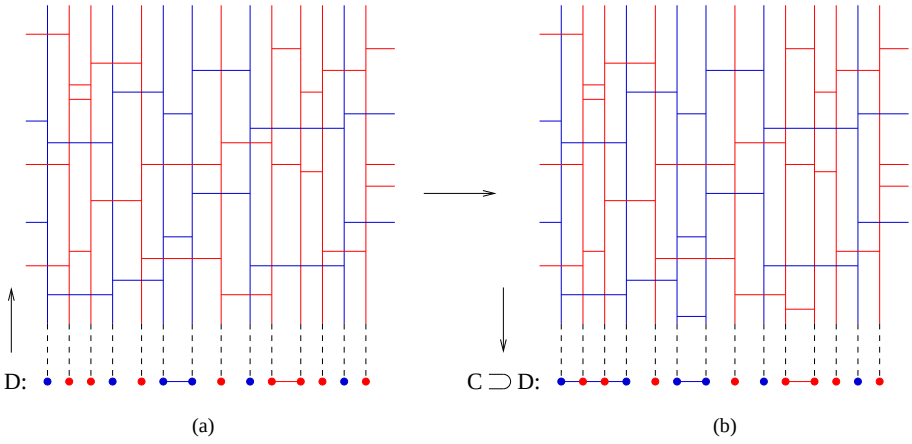

Figure 11: By completing an arbitrary triangulation of our sandwich geometry with a hard-dimer configuration D (a), we build a larger triangulation (b) whose projection C contains D. With this procedure (with fixed D) we build all triangulations whose projection C contains D exactly once.

$$g(D) = \sum_C f(C)\zeta(C,D) \tag{A-10}$$

with

$$g(D) = u^{|D|_b}v^{|D|_r}w^{|\cap D|}Z_{S_N}(u,v,w), \tag{A-11}$$

$$f(C) = u^{|D|_b}v^{|D|_r}w^{|\cap D|}Z^{(C)}_{S_N}(u,v,w), \tag{A-12}$$

and

$$\zeta(C,D) = \begin{cases} 1 & \text{if } C\supset D, \\ 0 & \text{otherwise.} \end{cases} \tag{A-13}$$

Thinking of the space of configurations as a vector space in this manner, (A-9) can be thought of as a vector-matrix multiplication, with an upper-triangular matrix $\zeta(C,D)$ and with all diagonal elements being equal to 1. Then ζ has an inverse matrix $\mu(D,C)$ of the form

$$\mu(D,C) = \begin{cases} (-1)^{|D|-|C|} & \text{if } D\supset C, \\ 0 & \text{otherwise.} \end{cases} \tag{A-14}$$

This property can be verified by noting that

$$\sum_D \zeta(C,D)\mu(D,C') = \begin{cases} \sum_{\substack{D\supset C'\\ D\subset C}} (-1)^{|D|-|C|} & \text{if } C\supset D\supset C', \\ 0 & \text{otherwise,} \end{cases} \tag{A-15}$$

and

$$\sum_{\substack{D\supset C'\\ D\subset C}} (-1)^{|D|-|C|} = \begin{cases} 1 & \text{if } C=C', \\ \sum_{i=0}^{|C|-|C'|}(-1)^i \binom{|C|-|C'|}{i} = (1-1)^{|C|-|C'|} = 0 & \text{otherwise.} \end{cases} \tag{A-16}$$

We can now invert (A-9) as[24]

$$u^{|C|_b} v^{|C|_r} w^{|\cap C|} Z^{(C)}_{S_N}(u,v,w) = \sum_{D\supset C} (-1)^{|D|-|C|} u^{|D|_b} v^{|D|_r} w^{|\cap D|} Z_{S_N}(u,v,w). \tag{A-17}$$

Noting that $Z_{S_N}(u,v,w)$ factors out of the sum on the right-hand side, we finally get

$$Z_{S_N}(u,v,w) = \frac{(-u)^{|C|_b}(-v)^{|C|_r} w^{|\cap C|} Z^{(C)}_{S_N}(u,v,w)}{\sum\limits_{D\supset C} (-u)^{|D|_b}(-v)^{|D|_r} w^{|\cap D|}}, \tag{A-18}$$

where we have used that $|D| = |D|_b + |D|_r$, leading to the minus sign in front of both u and v. Picking $C = \emptyset$, we arrive at the fundamental inversion relation (eq. (19) above)

$$Z_{S_N}(u,v,w) = \frac{1}{Z^{hcd}_{S_N}(-u,-v,w)}, \tag{A-19}$$

where

$$Z^{hcd}_{S_N}(u,v,w) = \sum_{\text{hard dimer config. } D} u^{|D|_b} v^{|D|_r} w^{|\cap D|} \tag{A-20}$$

denotes the partition function for hard coloured dimers with fugacity u (v) per blue (red) dimer and weight w per crossing.

A-III Numerical computations

A direct numerical computation of the generalized Lyapunov exponents L_n, defined in (44) above, is possible following the procedure given in [31]. One extracts a large number of values of γ at fixed N, computes the average $\langle e^{n\gamma N}\rangle$, and plots $L_n(N) = N^{-1}\ln\langle e^{n\gamma N}\rangle$ as a function of $1/N$. Usually $L_n(N)$ turns out to be linear in $1/N$ for large N,

$$L_n(N) \sim L_n + A_n/N, \tag{A-21}$$

which allows for a good extrapolation of the data to $N=\infty$, see Fig. 12 for an example. The values of γ are extracted as follows [31]:

1. construct a random unimodular vector v (e.g. by extracting the components from a Gaussian distribution);
2. extract the numbers q_j and apply the matrix M_{q_j} to v to obtain a vector $v' = \prod_j M_{q_j} v$;
3. compute $|v'| \simeq e^{N\gamma}$, which holds to leading order since the modulus of v' is dominated by the same largest eigenvalue of $\prod_j M_{q_j}$ which also dominates $\mathrm{Tr}\prod_j M_{q_j}$.

[24] This is the famous Möbius inversion formula of the theory of partially ordered sets, and μ is the associated Möbius function.

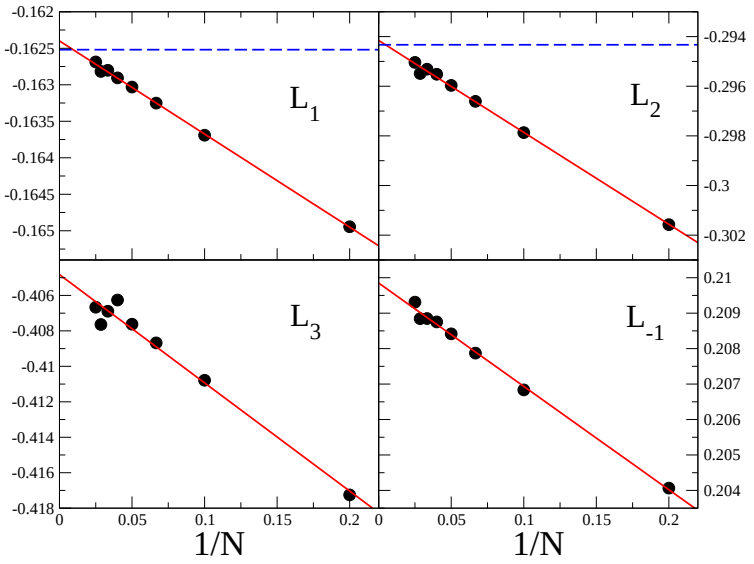

Figure 12: The numerical results for $L_n(N)$, $n = -1, 1, 2, 3$, as a function of $1/N$ for $u = 0.24$ and $w = 0.1$. The full lines are fits to $L_n(N) = L_n + A_n/N$. The dashed lines are the analytical values for L_1 and L_2 computed using the replica trick. They differ from the extrapolation by about 0.1%.

By repeating this procedure with random choices of the $\{q_j\}$, we obtain a set of $\mathcal{N}$ values γ_i, from which we can construct a histogram $\pi(\gamma)$ and extract the function $S(\gamma)$ at given N, see Fig. 8. The coincidence of the curves for different N indicates that the asymptotic limit $N \to \infty$ has been reached. To compute L_n, we first have to compute the average of γ, $\bar{\gamma} = \frac{1}{\mathcal{N}} \sum_{i=1}^{\mathcal{N}} \gamma_i$, and then use

$$e^{NL_n(N)} = \langle e^{n\gamma N} \rangle = e^{n\bar{\gamma}N} \frac{1}{\mathcal{N}} \sum_{i=1}^{\mathcal{N}} e^{nN(\gamma_i - \bar{\gamma})} \quad \Leftrightarrow \quad L_n(N) = n\bar{\gamma} + \frac{1}{N} \ln \left[\frac{1}{\mathcal{N}} \sum_{i=1}^{\mathcal{N}} e^{nN(\gamma_i - \bar{\gamma})} \right]. \tag{A-22}$$

By subtracting $\bar{\gamma}$ we can compute the average as long as the quantity $N(\gamma_i - \bar{\gamma}) \sim \sqrt{N}$ is not too large. In practice we are limited to $N < 50$, but this is enough to get a very good linear extrapolation to the limit $N \to \infty$. The difference between the numerical computation and the exact analytic expressions for L_1 and L_2 is of the order of 10^{-4}, see Fig. 12. We believe that a similar error affects the computation of L_{-1} too.

A-IV Fractional derivatives and inverse Laplace transforms

Although the notion of *fractional calculus* may at first appear somewhat extravagant, this is an old and well-studied subject in mathematics, with plenty of applications, as testified by the number of books on the subject (see, for instance, the list of references in [36, 37]). At the heart of the theory of fractional calculus is the definition and study of two operators $J^\alpha : f(x) \to J_x^\alpha f(x)$ and $D^\alpha : f(x) \to D_x^\alpha f(x)$ on a sufficiently large class of functions $\{f(x)\}$ and for a positive real number α, with the following properties.

1. When $\alpha = n$ is a positive integer, the operator J_x^α gives the same result as n-fold integration, and D_x^α gives the same result as the usual n-th derivative $\frac{d^n}{dx^n}$.

2. The operators of order $\alpha = 0$ are the identity operator.

3. J_x^α and D_x^α are linear operators.

4. For any α, β, the semigroup property holds for J^α_x, namely, $J^\alpha_x J^\beta_x f(x) = J^{\alpha+\beta}_x f(x)$.

There are many inequivalent definitions of fractional derivative/integral satisfying these properties, which we are not going to review here. Instead, we will recall the definition and properties of the one that turns out to be relevant for our purposes, the so-called Weyl fractional derivative/integral. (Reference [38] has a short review, which also contains a clear explanation for why the various definitions are inequivalent.) The Weyl fractional integral is defined as[25]

$$J^\alpha_{x,\infty} f(x) = \frac{1}{\Gamma(\alpha)} \int_x^\infty dt f(t)(t-x)^{\alpha-1}. \tag{A-23}$$

The natural definition of the derivative operator would be to take $D^\alpha_{x,\infty} = J^{-\alpha}_{x,\infty}$ but this is divergent. A standard trick is then to define

$$D^\alpha_{x,\infty} f(x) = \frac{d^{[\alpha]+1}}{dx^{[\alpha]+1}}\ J^{[\alpha]+1-\alpha}_{x,\infty} f(x), \tag{A-24}$$

where $[\alpha]$ is the integer part of α. The rationale behind this definition is that in this way D^α_x is the left inverse of J^α_x, *i.e.* $D^\alpha_x J^\alpha_x f(x) = f(x)$, the same as when $\alpha = n$ is an integer. With this definition it can be checked that

$$D^\alpha_{x,\infty} e^{-Ax} = (-1)^{[\alpha]+1} A^\alpha e^{-Ax}, \tag{A-25}$$

which, apart from the sign, is exactly what we need, as explained in the main text. According to the analysis there, we need to compute

$$\tilde{Z}(x, y, \Delta t = 1) = D^{1/4}_{\ln x,\infty} D^{1/4}_{\ln y,\infty} Z(x, y, \Delta t = 1)\ , \tag{A-26}$$

which in the continuum limit we can write as (see Sec. 9)

$$\tilde{Z}(X, Y) = D^{1/4}_{a^2 X,\infty} D^{1/4}_{a^2 Y,\infty} a^2 Z(X, Y) = a\ D^{1/4}_{X,\infty} D^{1/4}_{Y,\infty} Z(X, Y). \tag{A-27}$$

To leading order in a, we expect the transfer matrix to be given by the delta function $\delta(A_1 - A_2)$, which implies that we can simply take a $\frac{1}{2}$-derivative with respect to one of the arguments. From expression (86) for $Z(X, Y)$ we have

$$\begin{aligned} a D^{1/2}_{X,\infty} Z_{l.o.}(X, Y) &= D^{1/2}_{X,\infty} \frac{2}{\sqrt{X+Y}} = \lim_{X_0\to\infty} \frac{d}{dX} \frac{1}{\Gamma(1/2)} \int_X^{X_0} dt \frac{2}{\sqrt{t+Y}} \frac{1}{\sqrt{t-X}} \\ &= -\frac{2}{\sqrt{\pi}} \frac{1}{X+Y}, \end{aligned} \tag{A-28}$$

at leading order (*l.o.*), which is proportional to the Laplace transform of the delta function. Note that the limit has to be taken after the derivative, since otherwise it would be divergent. This is the kind of convergence problem mentioned in Sec. 8 (which by the way would remain if we used two $\frac{1}{4}$- instead of one $\frac{1}{2}$-derivative). It is not a real problem because all we need is an operator which gives the same result as (A-25) when acting on exponential functions. Since for exponential functions the limit can be taken both before and after the derivative, we have a freedom in choosing the order of these operations.

For the cosmological term in (86), interchanging limit and derivative is unproblematic and leads to

$$D^{1/4}_{X,\infty} D^{1/4}_{Y,\infty} \frac{-a\Lambda}{(X+Y)^{3/2}} = -\frac{2a}{\sqrt{\pi}} \frac{1}{(X+Y)^2}, \tag{A-29}$$

which is proportional[26] to the Laplace transform of $a\Lambda A_1 \delta(A_1 - A_2)$.

[25] The subscript "∞" refers to the extremum of integration. Other choices of extremum would give rise to different (and inequivalent) definitions of fractional derivative/integral, which we would denote by J^α_{x,x_0}, D^α_{x,x_0}.

[26] Note that although we obtained the same proportionality factor $-2/\sqrt{\pi}$ for both the identity and the cosmological term, there is a relative sign between the two because in the first case we used only one derivative, resulting in a minus sign (from the minus sign in (A-25)). If this sign difference was not there, we would have a negative effective cosmological constant.

For the remaining term in (86) we again must take the limit after the derivative, yielding

$$D^{1/4}_{X,\infty} D^{1/4}_{Y,\infty} a \left(\frac{5}{6} + \frac{XY}{(X+Y)^2} \right) = a \frac{\sqrt{\pi}(X^2 - 10XY + Y^2)}{16(X+Y)^{5/2}}, \tag{A-30}$$

with no contribution from the constant term. The inverse Laplace transform of this term gives another divergence. This may be avoided by an integration by parts, but we prefer to take another route and use the second method presented in Sec. 8. This consists in performing the inverse Laplace transform on $Z(X,Y)$ directly, without use of fractional derivatives, and then recognizing the contribution of the entropy in the Hamiltonian. Let us first see how this works for the leading-order term. We have to compute the integral

$$\begin{aligned} I(A_1, A_2) &\equiv \int_{-i\infty+\mu}^{+i\infty+\mu} \frac{dX}{2\pi i} e^{XA_1} \int_{-i\infty+\mu}^{+i\infty+\mu} \frac{dY}{2\pi i} e^{YA_2} \frac{2}{\sqrt{X+Y}} = \\ &= \int_{-i\infty+\mu}^{+i\infty+\mu} \frac{dY}{2\pi i} e^{Y(A_2-A_1)} \int_{-i\infty+\mu}^{+i\infty+\mu} \frac{dZ}{2\pi i} e^{ZA_1} \frac{2}{\sqrt{Z}} = \\ &= \delta(A_2 - A_1) \int_{-i\infty+\mu}^{+i\infty+\mu} \frac{dZ}{2\pi i} e^{ZA_1} \frac{2}{\sqrt{Z}}. \end{aligned} \tag{A-31}$$

Because of the square root, the integrand has a branch-cut along the semi-axis of negative Z. The usual Bromwich contour for the Laplace inversion therefore has to be continued along a Hankel contour around the cut, as shown in Fig. 13. We have

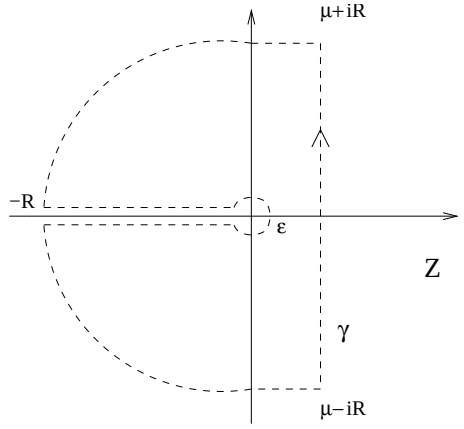

Figure 13: The Bromwich-Hankel contour used for the inverse Laplace transform. Integrating the function $e^{ZA_1}/\sqrt{Z}$ along this contour, we obtain (A-32) in the limit $R \to \infty$, $\epsilon \to 0$.

$$\begin{aligned} I(A_1, A_2) &= \delta(A_2 - A_1) \left(- \int_{-\infty^+}^{0^+} \frac{dZ}{2\pi i} e^{ZA_1} \frac{2}{i\sqrt{-Z}} - \int_{0^-}^{-\infty^-} \frac{dZ}{2\pi i} e^{ZA_1} \frac{2}{-i\sqrt{-Z}} \right) = \\ &= \delta(A_2 - A_1) \int_0^{+\infty} \frac{dZ'}{\pi} e^{-Z'A_1} \frac{2}{\sqrt{Z'}} = \frac{2}{\sqrt{\pi}} \frac{\delta(A_2 - A_1)}{\sqrt{A_1}}, \end{aligned} \tag{A-32}$$

in which we can recognize the subleading behaviour of (74). Multiplying by $\sqrt{A_1}$, we obtain exactly the same result as from the fractional derivative (apart from the sign arising in (A-25)).

For the cosmological term we have again a convergence problem, because instead of the square root in the denominator we have a power of 3/2, which diverges too fast at zero. This can be removed by a formal integration by parts in the previous step, and the final result coincides with that of the fractional derivative.

The remaining terms instead do not cause any problems. The constant term gives a term proportional to $\delta(A_1)\delta(A_2)$, which is a non-propagating and non-universal term of the kind already familiar from two dimensions (see [18] and references therein), and which furthermore gives just zero when multiplied by the inverse entropy factors $A_1^{1/4}A_2^{1/4}$, in agreement with the fractional derivative result. The last term has no branch-cut, and is the usual term encountered in two dimensions (see, for example, [9]). After an inverse Laplace transform it leads to an expression

$$\hat{H}''_{kin}\delta(A_2 - A_1) = \left(-A_2\frac{\partial^2}{\partial A_2^2} - \frac{\partial}{\partial A_2}\right)\delta(A_2 - A_1). \tag{A-33}$$

Dividing $\hat{H}''_{kin}$ by the entropy factor $1/\sqrt{A_2}$, we find the kinetic part of the auxiliary Hamiltonian (77), namely,

$$\hat{H}'_{kin} = -A_2^{\frac{3}{2}}\frac{\partial^2}{\partial A_2^2} - A_2^{\frac{1}{2}}\frac{\partial}{\partial A_2}. \tag{A-34}$$

Finally, by use of (78) (where $\mathcal{N}(A)$ has to be replaced by the subleading term of (74) only, because the exponential part is absorbed in the critical value of the boundary cosmological constants), we find the kinetic term of the final Hamiltonian (87).

As we have demonstrated in this appendix, the convergence problems encountered in the two methods are complementary, in the sense that the only problem with the auxiliary Hamiltonian method arises in the cosmological term, which instead presents no problems with regard to the fractional derivative.

References

[1] J. Ambjørn, R. Loll: *Non-perturbative Lorentzian quantum gravity, causality and topology change*, Nucl. Phys. B 536 (1998) 407-434 [hep-th/9805108].

[2] J. Ambjørn, J. Jurkiewicz, R. Loll: *Dynamically triangulating Lorentzian quantum gravity*, Nucl. Phys. B 610 (2001) 347-382 [hep-th/0105267].

[3] R.M. Williams: *Recent progress in Regge calculus*, Nucl. Phys. B (Proc. Suppl.) 57 (1997) 73-81 [gr-qc/9702006].

[4] R. Loll: *Discrete approaches to quantum gravity in four dimensions*, Living Rev. Rel. 1 (1998) 13, http://www.livingreviews.org [gr-qc/9805049]

[5] J. Ambjørn, J. Jurkiewicz, R. Loll: *The universe from scratch*, Contemp. Phys. 47 (2006) 103-117 [hep-th/0509010].

[6] J. Ambjørn, R. Loll, J.L. Nielsen, J. Rolf: *Euclidean and Lorentzian quantum gravity: Lessons from two dimensions*, Chaos Solitons Fractals 10 (1999) 177-195 [hep-th/9806241].

[7] P. Di Francesco, E. Guitter, C. Kristjansen: *Integrable 2d Lorentzian gravity and random walks*, Nucl. Phys. B 567 (2000) 515-553 [hep-th/9907084].

[8] J. Ambjørn, J. Correia, C. Kristjansen, R. Loll: *The relation between Euclidean and Lorentzian 2D quantum gravity*, Phys. Lett. B 475 (2000) 24-32 [hep-th/9912267].

[9] P. Di Francesco, E. Guitter, C. Kristjansen: *Generalized Lorentzian triangulations and the Calogero Hamiltonian*, Nucl. Phys. B 608 (2001) 485-526 [hep-th/0010259].

[10] R. Loll, W. Westra: *Sum over topologies and double-scaling limit in 2D Lorentzian quantum gravity*, Class. Quant. Grav. 23 (2006) 465-472 [hep-th/0306183].

[11] R. Loll, W. Westra and S. Zohren: *Taming the cosmological constant in 2D causal quantum gravity with topology change*, Nucl. Phys. B 751 (2006) 419-435 [hep-th/0507012].

[12] J. Ambjørn, J. Jurkiewicz and R. Loll: *Emergence of a 4D world from causal quantum gravity*, Phys. Rev. Lett. 93 (2004) 131301 [hep-th/0404156].

[13] J. Ambjørn, J. Jurkiewicz, R. Loll: *Semiclassical universe from first principles*, Phys. Lett. B 607 (2005) 205-213 [hep-th/0411152].

[14] J. Ambjørn, J. Jurkiewicz, R. Loll: *Spectral dimension of the universe*, Phys. Rev. Lett. 95 (2005) 171301 [hep-th/0505113].

[15] J. Ambjørn, J. Jurkiewicz, R. Loll: *Reconstructing the universe*, Phys. Rev. D 72 (2005) 064014 [hep-th/0505154].

[16] C. Bartocci, U. Bruzzo, M. Carfora, A. Marzuoli: *Entropy of random coverings and 4-d quantum gravity*, J. Geom. Phys. 18 (1996) 247-294 [hep-th/9412097].

[17] J. Ambjørn, M. Carfora, D. Gabrielli, A. Marzuoli: *Crumpled triangulations and critical points in 4D simplicial quantum gravity*, Nucl. Phys. B 542 (1999) 349-394 [hep-lat/9806035].

[18] J. Ambjørn, J. Jurkiewicz, R. Loll, G.Vernizzi: *Lorentzian 3d gravity with wormholes via matrix models*, JHEP 0109 (2001) 022 [hep-th/0106082].

[19] J. Ambjørn, J. Jurkiewicz, R. Loll: *Renormalization of 3d quantum gravity from matrix models*, Phys. Lett. B 581 (2004) 255-262 [hep-th/0307263].

[20] J. Ambjørn, J. Jurkiewicz, R. Loll, G.Vernizzi: *3D Lorentzian quantum gravity from the asymmetric ABAB matrix model*, Acta Phys. Polon. B 34 (2003) 4667-4688 [hep-th/0311072].

[21] V.A. Kazakov, P. Zinn-Justin: *Two-matrix model with ABAB interaction*, Nucl. Phys. B 546 (1999) 647-668 [hep-th/9808043].

[22] P. Zinn-Justin: *The asymmetric ABAB matrix model*, Europhys. Lett. 64 (2003) 737-742 [hep-th/0308132].

[23] B. Dittrich, R. Loll: *Counting a black hole in Lorentzian product triangulations*, Class. Quant. Grav. 23 (2006) 3849-3878 [gr-qc/0506035].

[24] S. Carlip: *Quantum gravity in 2+1 dimensions*, Cambridge University Press (1998).

[25] A. Dasgupta, R. Loll: *A proper-time cure for the conformal sickness in quantum gravity*, Nucl. Phys. B 606 (2001) 357-379 [hep-th/0103186].

[26] J. Ambjørn, J. Jurkiewicz, R. Loll: *Non-perturbative 3d Lorentzian quantum gravity*, Phys. Rev. D 64 (2001) 044011 [hep-th/0011276].

[27] B. Dittrich, R. Loll: *A hexagon model for 3d Lorentzian quantum cosmology*, Phys. Rev. D 66 (2002) 084016 [hep-th/0204210].

[28] P. Di Francesco, E. Guitter: *Critical and multicritical semi-random* $(1+d)$*-dimensional lattices and hard objects in d dimensions*, J. Phys. A 35 (2002) 897-927 [cond-mat/0104383].

[29] J. Polchinski: *String theory*, Cambridge University Press (1998).

[30] G. Viennot: *Heaps of pieces I: Basic definitions and combinatorial lemmas*, in G. Labelle and P. Lacroix, Eds, *Combinatoire Enumerative*, Lect. Notes in Math. 1234 (1986) 321-346.

[31] A. Crisanti, G. Paladin, A. Vulpiani: *Products of random matrices in statistical physics*, Springer-Verlag (1993).

[32] J. M. Deutsch, G. Paladin: *Product of random matrices in a microcanonical ensemble*, Phys. Rev. Lett. 62 (1989) 695-699.

[33] D. Benedetti: *Quantum gravity from simplices: analytical investigations on causal dynamical triangulations*, Doctoral Thesis, Utrecht University, June 2007.

[34] T. Regge: *General relativity without coordinates*, Nuovo Cim. 19 (1961) 558-571.

[35] J. B. Hartle, R. Sorkin: *Boundary terms in the action for the Regge calculus*, Gen. Rel. Grav. 13 (1981) 541-549.

[36] R. Gorenflo, F. Mainardi: *Fractional calculus: integral and differential equations of fractional order*, in *Fractals and fractional calculus in continuum mechanics*, (Udine, 1996), 223–276, CISM Courses and Lectures, 378, Springer, Wien (1997).

[37] http://www.tuke.sk/podlubny/fc_resources.html

[38] J.L. Lavoie, T.J. Osler, R. Tremblay: *Fractional derivatives and special functions*, SIAM Rev. 18 (1976) 240-268.